AWARD NUMBER: W81XWH-15-1-0613

TITLE: Fusing MRI and Mechanical Imaging for Improved Prostate Cancer Diagnosis

PRINCIPAL INVESTIGATOR: Dr. Mahdi Orooji

CONTRACTING ORGANIZATION:
Case Western Reserve University
Cleveland, Ohio 44106

REPORT DATE: December 2017

TYPE OF REPORT: Final

PREPARED FOR: U.S. Army Medical Research and Materiel Command
Fort Detrick, Maryland 21702-5012

REPORT DOCUMENTATION PAGE

Form Approved
OMB No. 0704-0188

1. REPORT DATE	2. REPORT TYPE	3. DATES COVERED
December 2017	Final	15 Sep 2015- 14 Sep 2017

4. TITLE AND SUBTITLE
Fusing MRI and Mechanical Imaging for Improved Prostate Cancer Diagnosis

5a. CONTRACT NUMBER

5b. GRANT NUMBER
W81XWH-15-1-0613

5c. PROGRAM ELEMENT NUMBER

6. AUTHOR(S)
Dr. Mahdi Orooji

E-Mail:mahdi.orooji@case.edu

5d. PROJECT NUMBER

5e. TASK NUMBER

5f. WORK UNIT NUMBER

7. PERFORMING ORGANIZATION NAME(S) AND ADDRESS(ES)
Western Reserve University
2071 Martin Luther King Drive
Cleveland, Ohio 44106-7207

8. PERFORMING ORGANIZATION REPORT NUMBER

9. SPONSORING / MONITORING AGENCY NAME(S) AND ADDRESS(ES)
U.S. Army Medical Research and Materiel Command
Fort Detrick, Maryland 21702-5012

10. SPONSOR/MONITOR'S ACRONYM(S)

11. SPONSOR/MONITOR'S REPORT NUMBER(S)

12. DISTRIBUTION / AVAILABILITY STATEMENT
Approved for Public Release; Distribution Unlimited

13. SUPPLEMENTARY NOTES

14. ABSTRACT
The main purpose of this project is to develop computerized fusion algorithms for combining a novel FDA approved imaging modality, prostate mechanical imaging (PMI), with multi-parametric MRI to improve the diagnosis of prostate cancer, especially in the context of repeat biopsies.

15. SUBJECT TERMS
Nothing listed

16. SECURITY CLASSIFICATION OF:			17. LIMITATION OF ABSTRACT	18. NUMBER OF PAGES	19a. NAME OF RESPONSIBLE PERSON
a. REPORT	b. ABSTRACT	c. THIS PAGE			USAMRMC
Unclassified	Unclassified	Unclassified	Unclassified	48	19b. TELEPHONE NUMBER *(include area code)*

Table of Contents

Page

Introduction:

This project serves to address the urgent need for marked improvement in prostate cancer (PCa) detection and diagnosis via the use of multimodal imaging for (a) biopsy planning and guidance, (b) PCa grading and staging, (c) active surveillance, and (d) treatment targeting and monitoring; due to severe limitations with current clinical protocol. For example, in May 2012 the US Preventive Task Force issued a recommendation against PSA based screening for PCa, concluding that it causes more harm than good. Current prostate biopsy procedures which primarily use conventional ultrasound (US) only have an estimated sensitivity of approximately 50%, with 90% of US-guided biopsies being negative. Similarly, focal therapy to treat PCa is gaining interest as a means of reducing toxic side effects, but it is unlikely to gain favor unless a reliable means of imaging and subsequently validating presence and extent of PCa is forthcoming.

A novel elastography tool, Prostate Mechanical Imaging (PMI) developed by Artann Labs, is newly FDA approved for PCa screening. Unlike conventional B-mode US, PMI allows for the measurement of gland volume and mechanical stress patterns on the gland surface through the rectal wall with pressure sensor arrays. However, PMI lacks the high spatial resolution of Magnetic Resonance Imaging (MRI). Multi-Parametric MRI (T2W, T1W, Diffusion, and DCE) has recently shown great promise for improving screening and detection of PCa as it provides significant structural and functional parameters for disease characterization. This project is to develop novel computerized fusion methods for precise registration of MRI and PMI in order to enable improved PCa detection in vivo compared to using either PMI or MRI alone. This research will have an impact on development of reliable and practical clinical means of imaging PCa for improved (1) biopsy planning and guidance, (2) grading and prognosis formulation, (3) active surveillance, (4) treatment planning, (5) disease targeting, and (6) treatment monitoring.

Keywords

Prostate Cancer, Radiomics, Magnetic Resonance Imaging, Prostate Mechanical Imaging, Digital Pathology, Computer Tomography Imaging, Intra-tumoral Texture Features, Shape Features, Vascular Features.

Accomplishments

Summary of Progress to Date:
The project has resulted in 1 submitted journal paper which recently received minor revision, 1 ready to submit journal papers, 4 peer reviewed abstracts, and 5 approved patent. All tasks proposed in this project have been completed by the end of the project period. Below we describe the specific progress performed under each of the original specific aims.

Milestone supposed to achieve in this project

- Conference such as SPIE Medical Imaging or International Symposium in Biomedical Imaging
    - Four abstracts were accepted on
        1- 24th International Society for Magnetic Resonance Medicine (ISMRM), 7-13 May 2016, Singapore.
        2- American Society of Clinical Oncology (ASCO) Annual Meeting, Jum 3-7 2016, Chicago, IL.
        3- 102nd Scientific Assembly and Annual Meeting of Radiological Society of North America (RSNA), Nov 27- Dec 3, Chicago, IL.
        4- 103rd Scientific Assembly and Annual Meeting of Radiological Society of North America (RSNA), Nov 26- Dec 1, Chicago, IL.

- A clinical imaging analysis journal such as Journal of Urology.
    - A journal on evaluating the computer extracted radiomics for discriminating the cancer from benign infection (Specific Aim 2, Task 1,2 and 3) a minor revision submitted to Journal of Medical Imaging (JMI)
    - A journal paper is in its final steps and is going to submit to Journal of Medical Imaging. The paper is in preparation on using the statistical shape model for the prostate segmentation (Specific Aim 1, Task 1)

- Registration techniques to align MRI, PMI, histology.
    - An algorithm is developed and presented on 24th International Society for Magnetic Resonance Medicine (ISMRM), 7-13 May 2016, Singapore.

- Methods to map cancer extent from histology (ground truth) onto radiology/mechanical imaging data to define signatures on *in vivo* imaging
    - An algorithm is developed and presented on 24th International Society for Magnetic Resonance Medicine (ISMRM), 7-13 May 2016, Singapore.

- Fusion and integrated visualization of mechanical and multi-parametric imaging data.
    - The achievements have been presented as an original research articles in:
        - American Society of Clinical Oncology (ASCO) Annual Meeting, Jum 3-7 2016, Chicago, IL.
        - 102nd Scientific Assembly and Annual Meeting of Radiological Society of North America (RSNA), Nov 27- Dec 3, Chicago, IL.
        - An algorithm is developed and presented on 24th International Society for Magnetic Resonance Medicine (ISMRM), 7-13 May 2016, Singapore.

- 103nd Scientific Assembly and Annual Meeting of Radiological Society of North America (RSNA), Nov 26- Dec 1, Chicago, IL

- Five US patents are granted in analyzing the medical image radiomics (textures and shape features) and the contribution of different radiomics in predicting pathologies.

Research-Specific Major Tast 1: Employing co-registration tools to align MP-MRI, PMI, *ex vivo* histologic sections

- **Aim 1-Task 1: Pre-processing of MP-MRI and histology,** Acquisition of multi-protocol *in vivo* MRI prostate data (T2w, DCE, DWI), prostate mechanical imaging data, with corresponding whole-mount histological (WMH) data from our collaborators.

My co-mentor Dr. Lee Ponsky, Urologist and professor in the University Hospital Case Medical Center (UHCMC), Case Western Reserve University accepted the primary responsibility to select cases for this project. Besides, Dr. Nicolas Bloch in Boston University School of Medicine, Boston, Massachusetts helped us by providing MRI and ultrasound of the prostate images. To develop the co-registration methodology for MRI-PMI fusion, we employed MRI-TRUS fusion algorithm. Table 1 shows the data we used in MRI-TRUS-WMH fusion.

Table 1: Acquired data for MRI-TRUS-WMH registration

Modality	MRI T1	MRI T2	Transrectal Ultrasound	Whole Mount Histological
Number of Studies	12	15	31	6

The main part of the pre-processing of the acquired data was focused on the prostate segmentation in the transrectal ultrasound. PI employed the statistical shape model for the prostate segmentation. A brief description and the results of employed method are as follows. The ongoing paper is attached in the appendices.

- *Spatial Statistic Aware Segmentation Paradigm: Application on the Prostate Segmentation in the Transrectal Ultrasound Images*

An accurate detection of the prostate volume and boundary is influential on diagnosis, treatment, and follow up of CaP. Within this framework, prostate segmentation on TRUS imagery is performed via introduced spatial statistic aware segmentation paradigm. The spatial prior probability is calculated in the training phase, and is used to estimate the texture feature parameters corresponding to the prostate and the background. Estimated parameters is employed to represent an alternative probabilistic presentation of the prostate in TRUS. Results show the 3D prostate capsule is more pronounced in the new representation which ultimately results in more accurate segmentation. Modified active shape model (ASM) is introduced and applied in the new 3D TURS representation for prostate segmentation. Figure 1 demonstrates the framework of the employed method.

Prostate segmentation in TRUS is a challenging task mainly due to the high inherent noise of the ultrasound images. On the other side, the proficiency of the texture features in the prostate segmentation is already investigated. We employed the power of the texture features in presenting the prostate in the ultrasound images and also the spatial statistics information to introduce an alternative representation. Figure 2 demonstrates the heatmap of the prostate and the background for Haralick features of the TRUS image, in which the prostate capsule is more pronounced in compare to the original TRUS image. We named it the TRUS-HeatMap Representation.

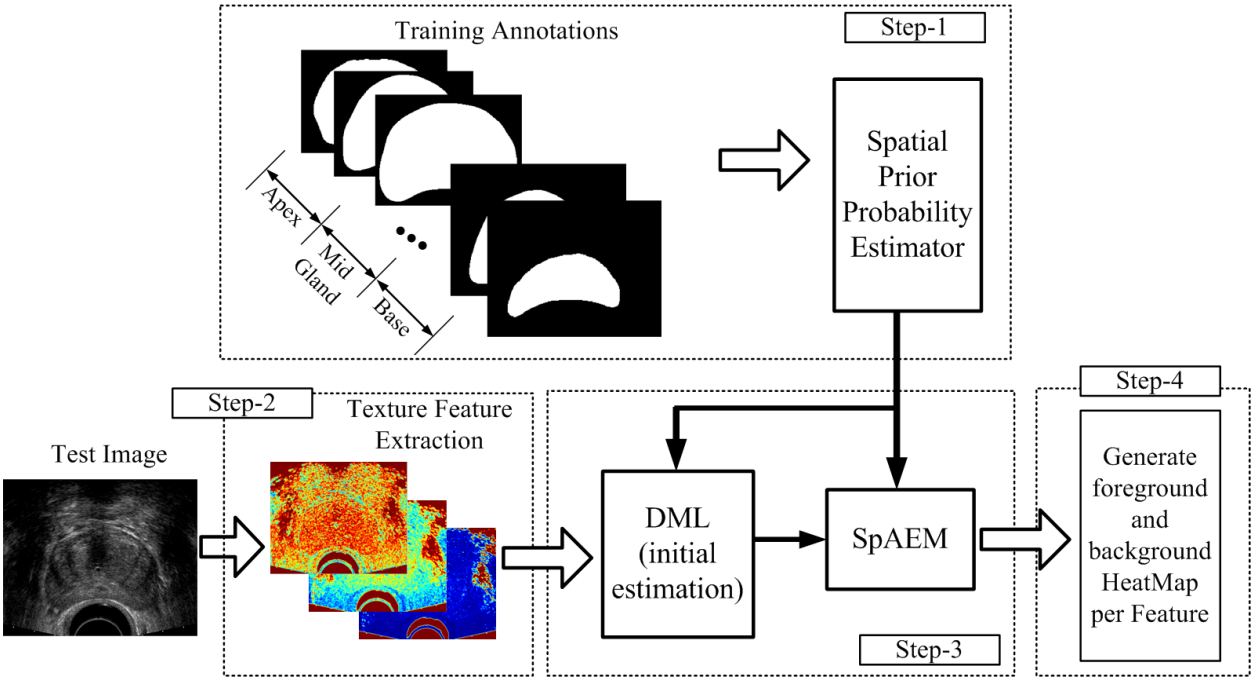

Figure 1: Schematic of four steps used for generating the foreground and background heat-map per texture feature.

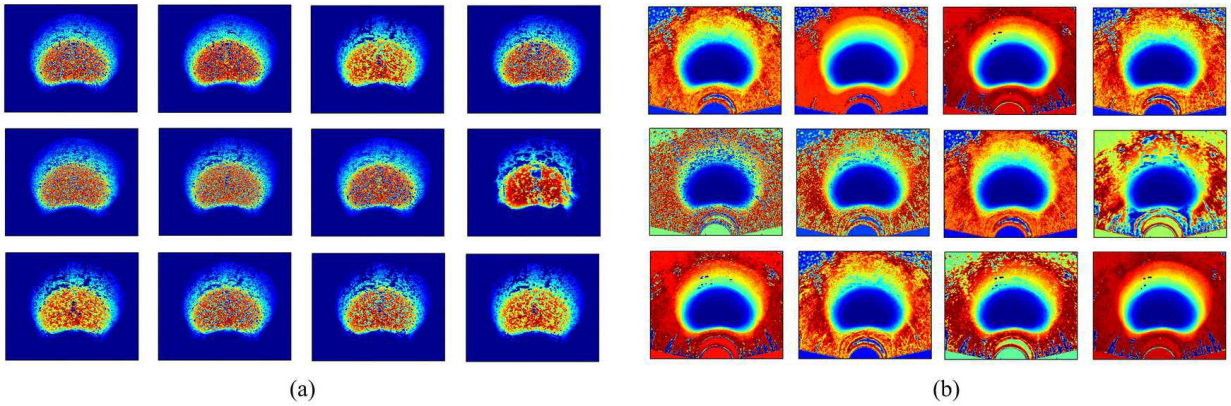

Figure 2. The probability heatmap of (a) the foreground probability and (b) the background probability.

- *Method used for PMI images:*

Prior to each PMI examination the probe is automatically calibrated by placing it into the calibrator. After this, a protective disposable sheath is placed over the PMI transrectal probe including the probe handle. A patient is asked to bend at a 90-degree angle at the hip for the PMI examination. The calibrated PMI probe covered by the sheath is lubricated and gently inserted into the anal canal with sensor surface facing downward. The probe is then gently inserted beyond the anal canal and into rectum until the axial projection of the prostate is visualized on the computer screen. The prostate scan is performed through a set of multiple manual compressions. The pressure sensor array, in response to input applied pressure, produces a pressure response map on a rectal wall covering the prostate, analogous to that sensed by the physician's finger palpating the prostate during DRE. The PMI provides 3-D pressure mapping of the prostate. This 3-D prostate map/image may be visualized and analyzed after the examination. Figure 3A demonstrates the real time cross-sectional images of the prostate obtained by PMI, and 3B is an actual prostate image of a patient obtained by PMI.

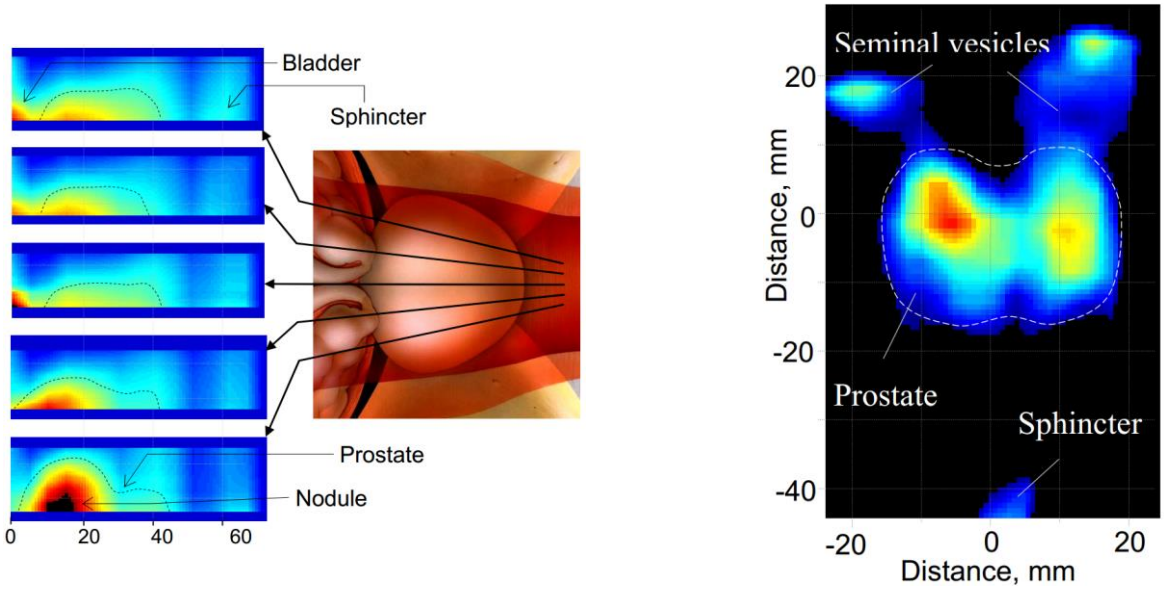

Figure 3. (A) Real time cross-sectional images of the prostate of a patient obtained by 5 successive pressings of the probe over the prostate at different location as shown in the picture. Patent data: PSA - 7.9; DRE - medium size asymmetrical prostate, left sided nodule, firm, immobile. PMI findings: hard nodule located at the prostate base in the left lobe. (B) An example of mechanical image of prostate of a patient.

- **Aim 1, Task 2: Co-registration of PMI with MP-MRI**

Subtask 1: Obtain a segmentation of the prostate on MP-MRI using the methodology Extract a set of features from the PMI capable of distinguishing between prostate tissue and non-prostate tissue.

The ROI was segmented in the previous step. A total of 645 2D texture and 24 3D-shape features were extracted from the segmented area. Texture features were extracted in 2D instead of 3D, since the available retrospective volumes were all anisotropic. After extracting per voxel based features within the nodule of interest, five statistics relating to mean, variance, minimum, maximum and the entropy were calculated. All feature calculations were implemented using MATLAB® 2014b platform (Mathworks, Natick, MA).

Subtask 2 and 3: Calculate a probabilistic model to estimate the prostate location on PMI and Apply an elastic registration to maximize the overlap between the MP-MRI segmentation and the PMI probabilistic model.

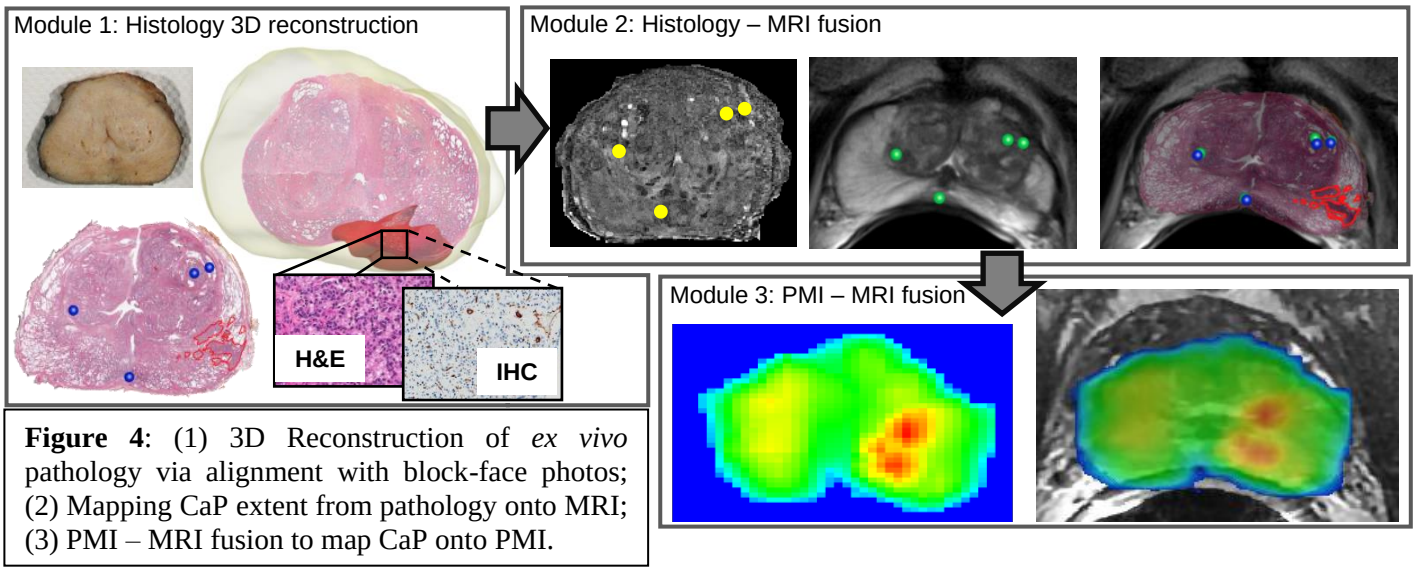

Figure 4: (1) 3D Reconstruction of *ex vivo* pathology via alignment with block-face photos; (2) Mapping CaP extent from pathology onto MRI; (3) PMI – MRI fusion to map CaP onto PMI.

Elastic registration methods developed in the mentor of the PI group in Case Western Reserve University yield a mapping of prostate cancer extent from *ex vivo* pathology on to corresponding MP-MRI, by allowing for recovery of non-linear deformations between the template and target images. PI extended our previous approaches by inclusion of additional imaging data to facilitate the registration: (1) block face photos of the *ex vivo* pathology, and (2) *ex vivo* MRI of the excised RP. The main steps are:

- Module 1: Reconstruct the 3D volume of the histopathology specimen, Path3D. This was involved (a) aligning the WMH slices to the block face section photos using 2D deformable registration, (2) applying groupwise registration to align block face pictures to each other; (3) implicitly reconstructing the 3D volume and providing a 3D volume for the tumor (see Figure 4).
- Module 2: 3D histology, Path3D, is aligned to the *ex vivo* MRI using 3D deformable co-registration. We then co-registered *ex vivo* to *in vivo* MRI using 3D deformable registration methods, such as finite element modeling (FEM). The transformation was constrained to physically meaningful deformations. Our approach determined optimal deformation forces that maximize similarity metrics based on MRI intensities. This will

allow for mapping of CaP annotation from histology on *in vivo* MRI. Figure 4 shows the result of registering WMH (IHC and H&E) to *in vivo* MRI via this technique.

Specific Aim 2: Evaluate an integrated MP-MRI/PMI for PCa diagnosis

To provide an optimize tool for MRI/PMI/WMH registration, PI developed MRI/TRUS/WMH registration algorithm. The method was published and presented in the 24th International Society for Magnetic Resonance Medicine (ISMRM), 7-13 May 2016, Singapore. The published abstract and the presented poster is attached in the appendices.

Subtask 3 of Aim 1: Evaluating PMI/MP-MRI/histology registration and Subtask 1 of Aim 2: Computerized extraction of MP-MRI features

Our study design comprised 12 2D planar images obtained from the MRI and US scans of 3 patients, all of whom had biopsy confirmed prostate cancer and scheduled for a radical prostatectomy. A 3D B-mode ultrasound scan was performed followed by a 3 Tesla MRI prior to surgery. Following surgery and histologic sectioning of the gland via a microtome, the H&E stained whole mount histologic (WMH) sections were digitized via a whole slide scanner and the regions of cancer annotated by an expert pathologist. Deformable co-registration methods were used to spatially align the *in vivo* MRI, TRUS, and ex vivo histology. In particular, we used fully automatic Multiattribute probabilistic prostate elastic registration (MAPPER) approach to fusion of ultrasound and MRI. We also manually delineated corresponding landmarks between MRI and WMH for deformable co-registration of WMH to MRI. A total of 129 computer extracted image features including Haralick, Gabor, Law, LBP, Laplacian features were extracted from both the prostate MRI and TRUS. Each of the computer extracted MRI and ultrasound features were then ranked via the Fisher criteria to identify the features that best identified the region of cancer. Figure 5 illustrates the MRI-TRUS-WMH registration and mapping of the cancer extent on MRI and TRUS.

Subtask 2 and 3: Computerized extraction and calibration of PMI features, and identifying the most discriminative features

The top 3 features for each modality and corresponding Fisher criteria values are shown in Table 4. The classification is per region of interest (ROI), i.e. the texture features for the cancerous part of the prostate is compared to the texture features of the noncancerous confounding regions. Top three texture features, contrast variance, contrast entropy, and contrast inverse moment were selected by the theoretical linear discriminant analysis (LDA) classifier for MRI and yielded an area under the receiver operating characteristic curve (AUC) of 0.83, 0.77 and 0.70 for identifying cancerous ROIs in MRI. By comparison, top three most predictive features identified for TRUS were contrast inverse moment, contrast variance, and contrast entropy. These features yielded an AUC of 0.75, 0.69, and 0.66, respectively. By combining the top two texture features on MRI and the most informative texture feature on TRUS, the LDA based predictor yielded an AUC of 0.88 in predicting presence of prostate cancer. Figure 6 illustrates the scatter plot of the prostate cancer versus the non-cancer cases in three dimensional most informative texture feature space.

The description of the extracted texture features and shape features can be found in Table 2 and Table 3.

Subtask 4: Evaluating the fused classifier

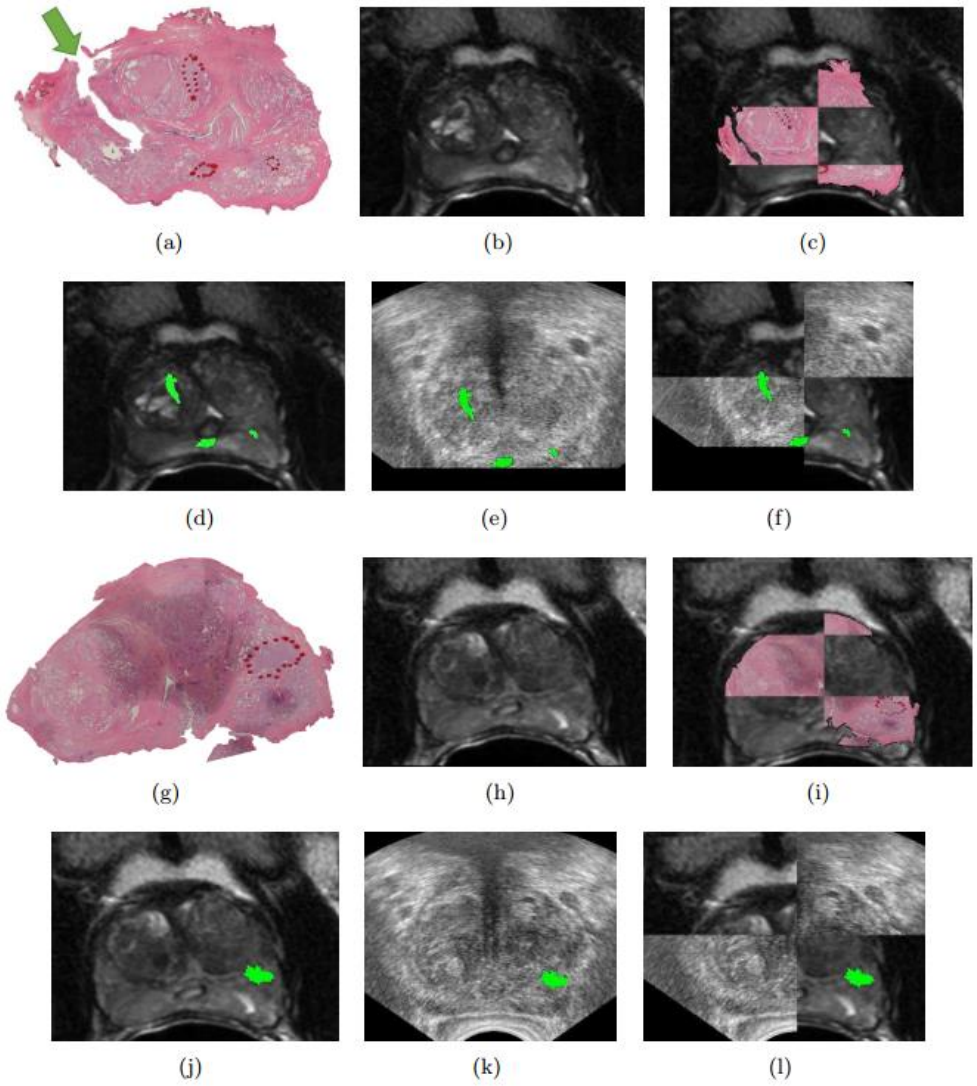

Figure 5: Registration of MRI, TRUS and WMH: Two 2D planar images of **(a),(g)** WMH and **(b),(h)** corresponding MRI. **(c),(i)** WMH and MRI checkerboard overlays showing alignment between the two modalities. **(d),(j)** MRI with cancer annotation obtained from WMH (green). **(e),(k)** TRUS with cancer annotation obtained from WMH (green). **(f),(l)** Fused MRI-TRUS images shown as checkerboards with cancer annotation obtained from WMH (green).

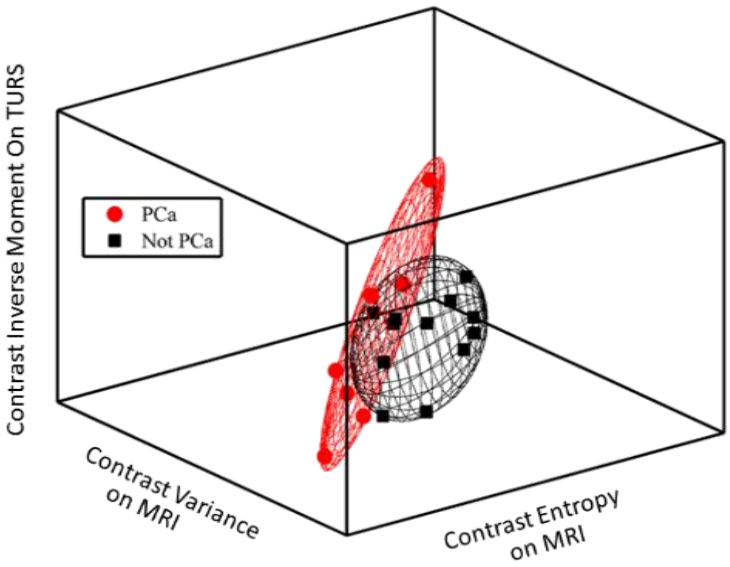

Figure 6: Scatter plot of three most discriminative texture features

Table 2: Texture features evaluated in this work.

Feature category	Descriptor	Intuitive Description
Haralick features (Repeated occurrence of grey level configuration in the texture represented via the grey-level co-occurrence matrix (GLCM), which varies rapidly with distance in fine textures and slowly in large textures)	Inverse Difference Moment (IDM)	IDM is a reflection of the presence or absence of uniformity, and hence is a measure of local regions of homogeneity High IDM: Higher presence of locally uniform windows in GLCM Low IDM: Higher presence of locally heterogeneous windows in GLCM
	Correlation	Quantifies the linear patterns in an image based on the distance parameter.
	Sum Entropy	Measure of GLCM relationship to distribution of intensity with respect to entropy. Entropy is the measure of disorder.
	Sum Variance	Measure of GLCM relationship to distribution of intensity with respect to variance High sum variance: greater standard deviation of sum average Low sum variance: low standard deviation of sum average

Laws features	E5, L5, S5,W5,R5 (combination in both *X* and *Y* directions)	E- Edges L- Level S- Spots W- Wave R- Ripple
Laplacian pyramids		Multi-resolution filters capture edges at different levels
Gray level features		The basic, intensity based features including mean, median, range and standard deviation.
Gabor Features		Oriented textures via changes in direction and scale; capture microarchitectures
Gradient Features		Represent the directional change in the intensity values of pixels in the ROI
Local Binary Pattern		Thresolding the window with the center pixel value.

Table 3: Shape features evaluated in this work.

Features	Description
Size	Including Width, Height, Depth of bounding box
Area	from 2D slices of each nodule
Perimeter	from 2D slices of each nodule
Eccentricity	foci of the ellipse and to major axis length
Extend	ratio of pixels in the region to pixels in the total bounding box
Compactness	ratio of the perimeter squared to the product of 4π and area
Radial distance	distances from center of each slice to contour points
Roughness	perimeter of slices divided by convex perimeter
Elongation	from major and minor axis
Convexity	from convex hull
Equivalent Diameter	Diameter of circle with same area of slices
Sphericity	3D compactness

Table 4: Top 3 features of MRI and TRUS, and their AUC values

Features for MRI	Contrast Variance	Contrast Entropy	Contrast. Inverse Moment
AUC	0.83	0.77	0.70
Features for TRUS	Contrast. Inverse Moment	Contrast Variance	Contrast Entropy
AUC	0.75	0.69	0.66

The ability of the PMI to discriminate abnormal prostates with nodules detected on DRE from normal prostates with normal DRE has been evaluated using Receiver Operating Characteristic (ROC) curve analysis. In the ROC curve (Figure 7) the true positive rate (sensitivity) is plotted as a function of the false positive rate (1-specificity) for different cut-off values of the "nodule detector" based on calculating maximum stress value inside the 3D prostate normalized image.

Each point on the ROC plot represents a sensitivity/specificity pair corresponding to a particular decision threshold. A test with perfect discrimination has a ROC plot that passes through the upper left corner, curve area equal to 100%. In our testing, the Area under the Curve (AUC) equals 78% with the 95% confidence interval from 65.7% to 87.7%. This means that a randomly selected individual from the positive group has a test value larger than that for a randomly chosen individual from the negative group in 78% of the time.

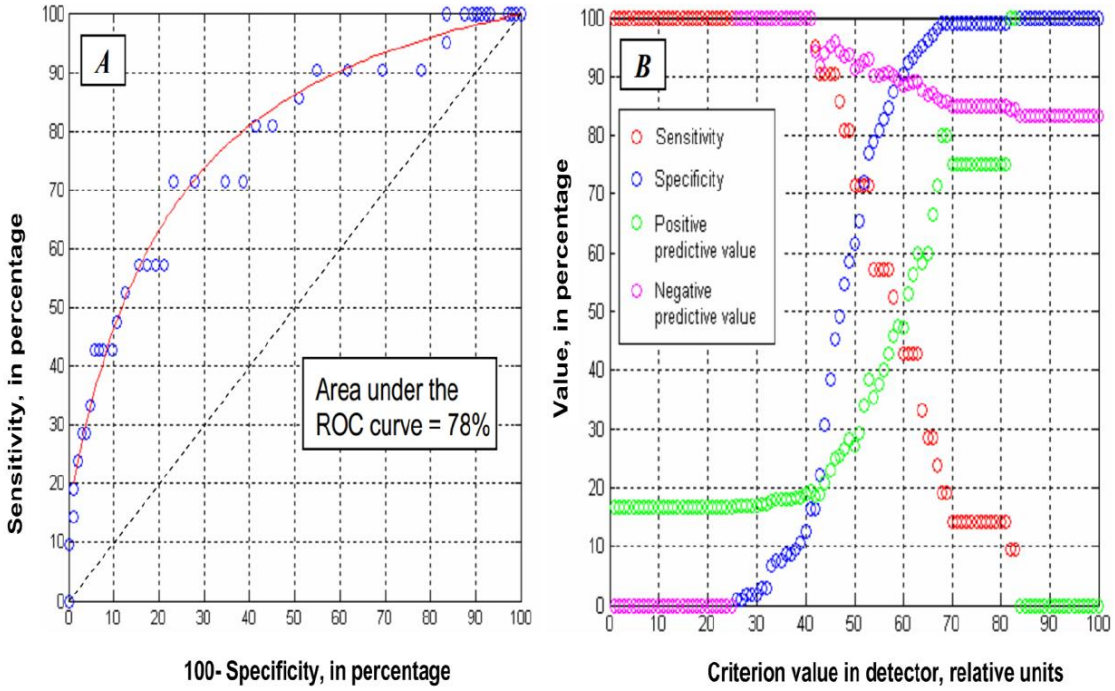

Figure 7: PMI nodule detection capability evaluated by Receiver Operating Characteristic (ROC) analysis. **(A)** ROC curve for nodule detection using PMI. **(B)** ROC parameters calculated for nodule detector output as a threshold value.

We evaluated the confidence interval for the ROC curve by modified fixed-width bands method. This is an acceptable result for a relatively simple classifier. Figure 7 shows sensitivity, specificity, and predictive values for the described test as a function of the threshold value. In the proximity of sensitivity/specificity interception, the graph shows that PMI sensitivity is 76% and specificity is 64%. The relatively low positive

This is a feasibility study to determine the clinical utility of Prostate Mechanical Imager for improved detection of prostate cancer. A total of 60 patients will be enrolled in this feasibility study. To ensure a meaningful difference can be discerned between patient's with low-risk prostate cancer from intermediate/high risk prostate cancer using the combination of PMI and MP-MRI, 30 patients with low risk disease and 30 patients with high risk disease will be included in the study. Prostate cancer risk is defined as per the National Comprehensive Cancer Network Guidelines as listed in Table 1 in Section 4.1 Inclusion Criteria.

Power analysis: The results from our preliminary studies show imaging features were able to distinguish prostate tumor level of risk with AUC about 0.79 (35). We expect the integration of MP-MRI and PMI will improve the accuracy of tumor level of risk classification with anticipated AUC in the ballpark of 0.91. With 30 low risk tumor grade and 30 patients with high risk, the power of the study is around 77%. The actual power depends on the true AUC obtained from the study. The figure below shows the relationship between power and various improvements of AUC (effect size).

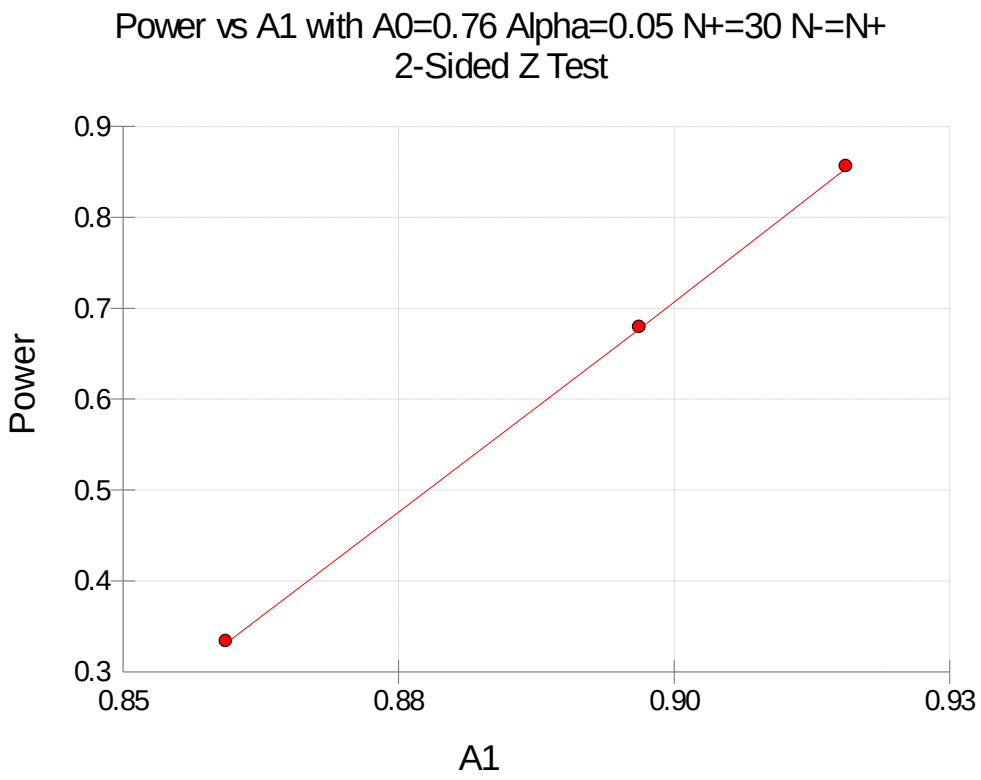

Training Specific Aims: Training and educational development in prostate cancer research.

Subtask 1: Mechanical Imaging Training session in Artann Labs (Two weeks in the first year and two weeks in the second year). The PI scheduled the first training session for the middle of December 2016.

Subtask 2: Seminars

- PI had weekly mentor lab meeting, in the Center for Computational Imaging and Personalized Diagnostics (CCIPD) at Case Western Reserve University.
- PI is participating weekly Prostate Imaging Reporting and Data System meeting in the Department of Radiology, Case Medical Center University Hospital with PI's mentor, clinical co-mentor and radiology collaborators.
- PI is participating the Biomedical Image Analysis Literary Guild (LG) seminar, Case Western Reserve University. Hosted by PI's mentor.
- PI is participating the majority of Imaging Hour meeting, Department of Biomedical Engineering, Case Western Reserve University.
- PI is participating the majority of monthly Cancer Center Seminar Series, Case Comprehensive Cancer Center.

Subtask 3: Course works

PI studied the course materials of "Cancer Biology, Immunology, and Pathology", and "Biostatistics".

Subtask 4: Attending a scientific meeting in relevant scientific field

- PI participated and also presented his works on
    - American Society of Clinical Oncology (ASCO) Annual Meeting, Jum 3-7 2016, Chicago, IL.
    - 102nd Scientific Assembly and Annual Meeting of Radiological Society of North America (RSNA), Nov 27- Dec 3, Chicago, IL.
    - 103rd Scientific Assembly and Annual Meeting of Radiological Society of North America (RSNA), Nov 26- Dec 1, Chicago, IL.

Impact

A novel elastography tool, Prostate Mechanical Imaging (PMI) developed by Artann Labs, is newly FDA approved for PCa screening. Unlike conventional B-mode US, PMI allows for the measurement of gland volume and mechanical stress patterns on the gland surface through the rectal wall with pressure sensor arrays. However, PMI lacks the high spatial resolution of Magnetic Resonance Imaging (MRI). Multi-Parametric MRI (T2W, T1W, Diffusion, and DCE) has recently shown great promise for improving screening and detection of PCa as it provides significant structural and functional parameters for disease characterization. This project developed novel computerized fusion methods for precise registration of MRI and PMI in order to enable improved PCa detection *in vivo* compared to using either PMI or MRI alone. This research have an impact on development of reliable and practical clinical means of imaging PCa for improved (1) biopsy planning and guidance, (2) grading and prognosis formulation, (3) active surveillance, (4) treatment planning, (5) disease targeting, and (6) treatment monitoring.

Changes/Problems
Nothing to report

Products

Accepted and presented abstracts:

- Mahdi Orooji, Mehdi Alilou, Rachel Sparks, Mirabela Rusu,B Nicolas Bloch, Ernest Feleppa, Dean Barratt, Lee Ponsky, Anant Madabhushi, "A Combination of Radiomic Features from MRI and Ultrasound Appears to better predict presence of prostate cancer: Validation against whole mount pathology", 24th International Society for Magnetic Resonance Medicine (ISMRM), 7-13 May 2016, Singapore.

- Orooji, M., Rakshit, S., Beig, N., Velcheti, V., Madabhushi, A., "Computerized textural analysis of lung CT enables quantification of tumor infiltrating lymphocytes in NSCLC", American Society for Clinical Oncology (ASCO) Annual Meeting, Chicago, IL, 2016

- Rakshit, S., Orooji, M., Beig, N., Velcheti, V., Madabhushi, A., "Use of radiomic features on baseline CT scan to predict clinical benefit for pemetrexed based chemotherapy in metastatic lung adenocarcinoma", American Society for Clinical Oncology (ASCO) Annual Meeting, Chicago, IL, 2016

- Mahdi Orooji, Mehdi Alilou, Niha Beig, Sagar Rakshit, Prabhakar Rajiah, Michael Yang, Frank Jacono, Robert Gilkeson, Philip Linden, Vamsidhar Velcheti, Anant Madabhushi, "A combination of shape and texture features enables discrimination of benign fungal infection from non-small cell lung adenocarcinoma on chest CT", 102nd Scientific Assembly and Annual Meeting of Radiological Society of North America (RSNA), Nov 27- Dec 3, Chicago, IL.

- Mahdi Orooji, Monica Khunger, Mehdi Alilou, Rajat Thawani, Vamsidhar Velcheti, Anant Madabhushi, " Nodule texture predicts Response to Nivolumab based immunotherapy for non-small cell lung cancer", 103rd Scientific Assembly and Annual Meeting of Radiological Society of North America (RSNA), Nov 26- Dec 1, Chicago, IL.

Ongoing Journal Article:

- Mahdi Orooji, Mehdi Alilou, Sagar Rakshit, Niha Beig, Mohammad Hadi Khorrami, Prabhakar Rajiah, Rajat Thawani, Jennifer Ginsberg, Christopher Donatelli, Michael Yang, Frank Jacono, Robert Gilkeson, Vamsidhar Velcheti, Philip Linden, Anant Madabhushi, "A Combination of Computer Extracted Shape and Texture Features Enables Discrimination of Granulomas from Adenocarcinoma on Chest CT", Minor revision submitted to Journal of Medical Imaging (JMI)

- Mahdi Orooji, Mehdi Alilou, Lee Ponsky, Anant Madabhushi, "Spatial Statistic Aware Segmentation Paradigm: Application on the Prostate Segmentation in the Transrectal Ultrasound Images", is going to submit to Journal of Medical Imaging.

US Patent

- Textural analysis of lung nodules

A Madabhushi, M Rusu, M Orooji, M Alilou
US Patent 9,595,103

- Decision support for disease characterization and treatment response with disease and peri-disease radiomics

A Madabhushi, M Orooji, M Rusu, P Linden, R Gilkeson, NM Braman
US Patent App. 15/226,124

- Characterizing disease and treatment response with quantitative vessel tortuosity radiomics

A Madabhushi, M Orooji, M Rusu, P Linden, R Gilkeson, NM Braman
US Patent App. 15/226,148

- Computerized analysis of computed tomography (ct) imagery to quantify tumor infiltrating lymphocytes (tils) in non-small cell...

A Madabhushi, V Velcheti, M Orooji, S Rakshit, M Alilou, N Beig
US Patent App. 15/613,751

- Predicting response to pemetrexed chemotherapy in non-small cell lung cancer (nsclc) with baseline computed tomography (...

A Madabhushi, V Velcheti, M Orooji, S Rakshit, M Alilou, N Beig
US Patent App. 15/612,467

Participants & Other Collaborating Organizations.

- What individuals have worked on the project?
  PI: Mahdi Orooji, PhD: No change
  Mentor: Anant Madabhushi, PhD: No change
  Co-mentor: Lee Ponsky, MD: No change
  Collaborator: Pingfu Fu, PhD: No change
  Collaborator: Vikas Gulani, MD: No change
  Collaborator: Raj Paspulati, MD: No Change
  Collaborator: Armen Sarvazian, PhD: No change
  Collaborator: Gregory MacLennan, MD: No change

- Has there been a change in the active other support of the PD/PI(s) or senior/key personnel since the last reporting period?
  Nothing to Report

- What other organizations were involved as partners?
  Nothing to Report

Special Reporting Requirements
Nothing to report

Appendices

Part 1: Accepted Papers

Abstract #171681

Computerized textural analysis of lung CT to enable quantification of tumor infiltrating lymphocytes in NSCLC.

Mahdi Orooji, Sagar Rakshit, Niha Beig, Anant Madabhushi, Vamsidhar Velcheti; Biomedical Engineering, Case Western Reserve University, Cleveland, OH; Cleveland Clinic Foundation, Cleveland, OH; Case Western Reserve University, Cleveland, OH; Cleveland Clinic, Cleveland, OH

Abstract Text:

Background: Tumor infiltrating lymphocytes (TILs) are a part of the dynamic immune microenvironment. Clinical trials with immune checkpoint inhibitors report significant increase in TILs in responders in follow up tumor biopsies. Monitoring TILs on treatment using radiomic features extracted from routine follow up computed tomographic (CT) images can be a non-invasive surrogate to biopsy to detect early response. We conducted a proof of concept study to find out if radiomic features extracted from CT images can identify patients with high and low TILs in non-small cell lung cancer (NSCLC).

Methods: A cohort of 50 consecutive patients who underwent lobectomy for early stage NSCLC were identified and TIL were characterized using routine hematoxylin and eosin (H&Es) slides. TILs were quantified on a previously reported scale of 0 to 3 based on intensity of TIL. Of the 50 cases 17 outliers who had high TILs (3+) or low TILs (0) were identified. The study team was provided with CT images from 4 patients with '0' TILs, 8 tumors with '3+' TILs and 5 tumors were blinded. Corresponding pre-surgical CT scans were annotated on slicer-3D software. A total of 669 radiomic (textural and shape) features of the lung nodule were investigated. These features were evaluated and ranked in their ability to discriminate TIL extent using a linear discriminant classifier, both in terms of univariate and multivariate analysis.

Results: Sphericity, a shape based feature was the most discriminating feature. Standard deviation and Laws were ranked as the most promising texture based features. Of the 5 blinded tumors, 4 were classified correctly leaving only one misclassified case.

Conclusions: Computerized textural analysis using shape and texture features extracted from the lung nodule on CT images could be used to identify tumors with high TILs. Further validation of these findings in larger independent cohorts is required. These novel imaging based biomarkers could be a useful diagnostic tool for predicting response and monitoring patients on immunotherapy.

Abstract #171139

Evaluation of radiomic features on baseline CT scan to predict clinical benefit for pemetrexed based chemotherapy in metastatic lung adenocarcinoma.

Sagar Rakshit, Mahdi Orooji, Niha Beig, Mehdi Alilou, Nathan A. Pennell, James Stevenson, Marc A. Shapiro, Anant Madabhushi, Vamsidhar Velcheti; Cleveland Clinic Foundation, Cleveland, OH; Biomedical Engineering, Case Western Reserve University, Cleveland, OH; Cleveland Clinic, Cleveland, OH; Case Western Reserve University, Cleveland, OH

Abstract Text:

Background: Many patients receiving standard of care pemetrexed based platinum doublet followed by maintenance pemetrexed for lung adenocarcinoma do not receive clinical benefit. Currently there are no clinically validated biomarkers to identify patients who benefit from these treatments. We conducted a retrospective proof-of concept study to identify predictive computer extracted image features from pre-treatment computed tomographic (CT) scans.

Methods: Pre-chemotherapy CT scans were obtained for 105 lung adenocarcinoma patients treated with pemetrexed based chemotherapy at the Cleveland Clinic from 2004-2010. Clinical benefit was defined as patients with an objective response or more than 12 cycles of pemetrexed therapy. We identified and annotated CT images in 2 groups- 46 with clinical benefit and 59 without clinical benefit. After adjusting for image quality and CT filters, 32 and 33 patients remained for final analysis in the 2 groups respectively. A total of 1108 radiomic features including both textural and shape features of the lung nodule as well as the peritumoral region were investigated. The features were evaluated and ranked in their ability to discriminate between the 2 groups in conjunction with a linear discriminant classifier, both in terms of univariate and multivariate analysis.

Results: Two of the top 3 ranked features were from within the nodule and the third was from within the peritumoral area. Mean of Sum Average, a co-occurrence based texture measure within the nodule was the most discriminating feature. Combination of features within and around the nodule yielded even higher AUC values (See Table for combination of best features).

Conclusions: Texture and shape features extracted from within and around the lung nodule on CT images could identify patients who could potentially benefit from pemetrexed based chemotherapy. Further validation in a larger retrospective, multi-institutional cohort is needed.

Feature Vector	Area Under ROC Curve ± Standard Deviation
Mean of Intratumoral Sum Average(1)	69.5% ± 3.0%
1+Minimum of Intratumoral Law L5xE5(2)	75.2% ± 3.2%
1+2+Mean of Peritumoral Law S5xW5(3)	77.6% ± 1.9%

A Combination of Radiomic Features from MRI and Ultrasound Appears to better predict presence of prostate cancer: Validation against whole mount pathology

Authors: Mahdi Orooji[1], Mehdi Alilou[1], Rachel Sparks[2], Mirabela Rusu[1],B Nicolas Bloch[3], Ernest Feleppa[4], Dean Barratt[2], Lee Ponsky[5], Anant Madabhushi[1]

[1] Center for Computational Imaging and Personalized Diagnostics, Case Western Reserve University, Cleveland, OH, USA

[2]Centre for Medical Image Computing, University College of London

[3]Boston University School of Medicine, Boston, Massachusetts

[4]Lizzi Center for Biomedical Engineering, Riverside Research

[5]University Hospital Case Medical Center, Case Western Reserve University, Cleveland, OH, USA

Synopsis:

To evaluate whether the combination of computer extracted or radiomic image parameters from two complementary modalities, MRI-Transrectal Ultrasound (TRUS) can enable better prediction of presence of prostate cancer compared to either modality individually. In order to evaluate the ability of the radiomic features from MRI and ultrasound and the combination of MRI and ultrasound radiomic features in predicting the presence of prostate cancer we considered 3 patients who underwent MRI, transrectal ultrasound prior to radical prostatectomy. Deformable co-registration methods were used for spatially aligning the pre-operative *in vivo* MRI and ultrasound with the *ex vivo* whole mount radical prostatectomy specimens to establish the "ground truth" for cancer extent on the imaging. A combination of texture features from US and MRI yielded the best separability between cancer and non-cancer regions with an Area under the operating characteristic curve of 0.88.

PURPOSE:

Recently there has been a great deal of interest in developing computer aided diagnosis systems for identifying prostate cancer presence *in vivo* on MRI and ultrasound

separately[1-3], no work we are aware of has attempted to address the issue of fusing computer derived features from MRI and ultrasound to create the best possible predictor of cancer in vivo. In this work we attempt a systematic and quantitative evaluation of the discriminability of computer extracted MRI and ultrasound features in terms of cancer detection in patients undergoing radical prostatectomy.

METHODS:

Our study design comprised 12 2D planar images obtained from the MRI and US scans of 3 patients, all of whom had biopsy confirmed prostate cancer and scheduled for a radical prostatectomy. A 3D B-mode ultrasound scan was performed followed by a 3 Tesla MRI prior to surgery. Following surgery and histologic sectioning of the gland via a microtome, the H&E stained whole mount histologic (WMH) sections were digitized via a whole slide scanner and the regions of cancer annotated by an expert pathologist. Deformable co-registration methods were used to spatially align the in vivo MRI, TRUS, and *ex vivo* histology. In particular, we used fully automatic Multiattribute probabilistic prostate elastic registration (MAPPER) approach to fusion of ultrasound and MRI[4]. We also manually delineated corresponding landmarks between MRI and WMH for deformable co-registration of WMH to MRI. A total of 129 computer extracted image features including Haralick, Gabor, Law, LBP, Laplacian features were extracted from both the prostate MRI and TRUS. Each of the computer extracted MRI and ultrasound features were then ranked via the Fisher criteria to identify the features that best identified the region of cancer. Figure 1 illustrates the MRI-TRUS-WMH registration and mapping of the cancer extent on MRI and TRUS.

RESULTS AND DISCUSSION

The top 3 features for each modality and corresponding Fisher criteria values are shown in Table.1. The classification is per region of interest (ROI), i.e. the texture features for the cancerous part of the prostate is compared to the texture features of the noncancerous confounding regions. Top three texture features, contrast variance, contrast entropy, and contrast inverse moment were selected by the theoretical linear discriminant analysis (LDA) classifier for MRI and yielded an area under the receiver operating characteristic curve (AUC) of 0.83, 0.77 and 0.70

for identifying cancerous ROIs in MRI. By comparison, top three most predictive features identified for TRUS were contrast inverse moment, contrast variance, and contrast entropy. These features yielded an AUC of 0.75, 0.69, and 0.66, respectively. By combining the top two texture features on MRI and the most informative texture feature on TRUS, the LDA based predictor yielded an AUC of 0.88 in predicting presence of prostate cancer. Figure 2 illustrates the scatter plot of the prostate cancer versus the non-cancer cases in three dimensional most informative texture feature space.

CONCLUSION:

We presented a framework to rank the performance of computer extracted MRI and ultrasound features in terms of their ability to identify prostate cancer. Our results in a small cohort suggests that we may be able to combine the MRI and ultrasound radiomic features to create a better classifier for prostate cancer detection compared to MRI or ultrasound alone.

References:

[1]Emilie Niaf, Olivier Rouvire, Florence Mge-Lechevallier, Flavie Bratan, Carole Lartizien," Computer-aided diagnosis of prostate cancer in the peripheral zone using multiparametric MRI", Physics in Medicine and Biology 2012.

[2]Tiwari P, Kurhanewicz J, Rosen M, Madabhushi A. (2010) Semi supervised multi kernel (SeSMiK) graph embedding: identifying aggressive prostate cancer via magnetic resonance imaging and spectroscopy. Med Image Comput Comput Assist Interv. 13(Pt 3):666-73

[3]Mehdi Moradi, Parvin Mousavi, Purang Abolmaesumi, Computer-Aided Diagnosis of Prostate Cancer with Emphasis on Ultrasound-Based Approaches: A Review, Ultrasound in Medicine & Biology, Volume 33, Issue 7, July 2007, Pages 1010-1028, ISSN 0301-5629

[4] Sparks, Rachel and Nicolas Bloch, B. and Feleppa, Ernest and Barratt, Dean and Moses, Daniel and Ponsky, Lee and Madabhushi, Anant, "Multiattribute probabilistic prostate elastic registration (MAPPER): Application to fusion of ultrasound and magnetic resonance imaging", Medical Physics, 42, 1153-1163 (2015),

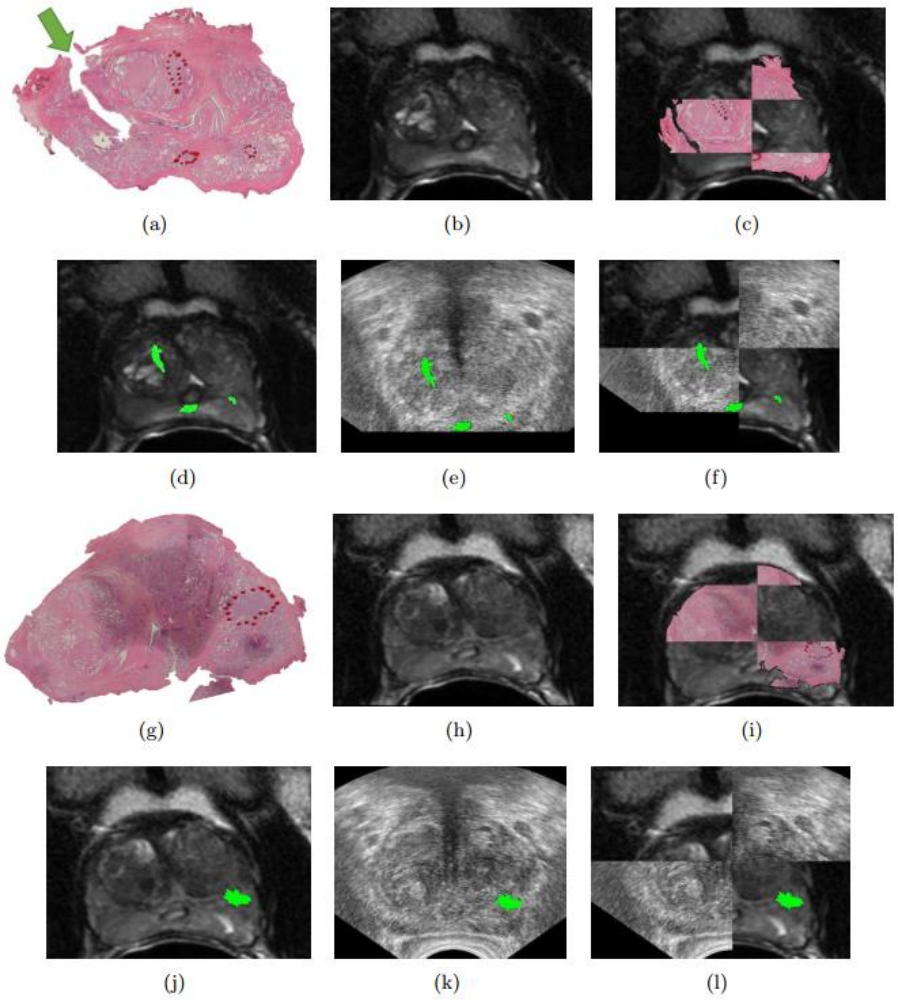

Figure 1: Registration of MRI, TRUS and WMH: Two 2D planar images of **(a),(g)** WMH and **(b),(h)** corresponding MRI. **(c),(i)** WMH and MRI checkerboard overlays showing alignment between the two modalities. **(d),(j)** MRI with cancer annotation obtained from WMH (green). **(e),(k)** TRUS with cancer annotation obtained from WMH (green). **(f),(l)** Fused MRI-TRUS images shown as checkerboards with cancer annotation obtained from WMH (green).

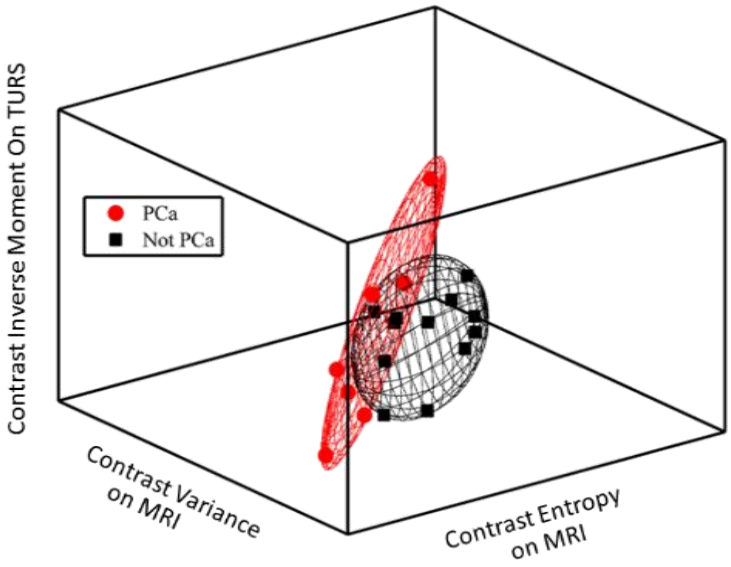

Figure 2: Scatter plot of three most discriminative texture features

Table 1: Top 3 features of MRI and TRUS, and their AUC values

		Entropy	Inverse Moment
AUC	0.83	0.77	0.70
Features for TRUS	Contrast. Inverse Moment	Contrast Variance	Contrast Entropy
AUC	0.75	0.69	0.66

Accepted paper in RSNA 2017:

Tuesday 10:30-12:00 PM | SSG03 | Room: S404CD
Mannudeep K. Kalra, MD | Mark L. Schiebler, MD

SSG03-07 **Nodule Texture Predicts Response to Nivolumab Based Immunotherapy for Non-Small Cell Lung Cancer**
Mahdi Orooji, PhD | Monica Khunger, MD | Mehdi Alilou, PhD | Rajat Thawani, | Vamsidhar Velcheti, MD | Anant Madabhushi, PhD

Nodule Texture Predicts Response to Nivolumab Based Immunotherapy for Non-Small Cell Lung Cancer

Tuesday 11:30-11:40 AM | SSG03-07 | Room: S404CD

PARTICIPANTS:

Mahdi Orooji, PhD Cleveland, OH **(Presenter)**
Disclosure: Nothing to Disclose
Monica Khunger, MD Cleveland, OH
Disclosure: Nothing to Disclose
Mehdi Alilou, PhD Cleveland, OH
Disclosure: Nothing to Disclose
Rajat Thawani, Cleveland, OH
Disclosure: Nothing to Disclose
Vamsidhar Velcheti, MD Saint Louis, MO
Disclosure: Nothing to Disclose
Anant Madabhushi, PhD Piscataway, NJ
Disclosure: Nothing to Disclose

PURPOSE

Nivolumab, a PD-1 inhibitor has shown clinical efficacy in patients with non-small cell lung cancer (NSCLC). It has been approved for treatment of patients with chemotherapy refractory, advanced NSCLC. The current standard clinical approach to evaluating tumor response is sub-optimal in defining clinical benefit from immunotherapy drugs. We sought to evaluate whether computer extracted radiomic features of nodule texture and shape from a baseline CT scan are predictive of response to nivolumab based immunotherapy.

METHOD AND MATERIALS

A cohort of 31 consecutive patients who were treated with nivolumab were included in the study. Patients who did not receive nivolumab after 2 cycles due to lack of response or progression as per RECIST were classified as 'non-responders'; patients who had radiological response per RECIST or had clinical benefit (defined as stable disease >10 cycles) were classified as 'responders'. The study team was provided with CT images from 10 patients who responded to nivolumab, 10 who did not and 11 Cases were blinded for validation. A total of 669 intra-tumoral texture (Gabor, Laws, Haralick) features were extracted and the top 4 features predictive of response on the training set (N = 20) were identified. Within the space of the top features, the optimal decision boundary for separating the training instances was identified via a Quadratic Discriminant Analysis (QDA) approach. The decision boundary was then used to evaluate the test cases (N = 11).

RESULTS

The top ranked features were the entropy, Kurtosis, and Variance of the Gabor texture feature and Variance of the Law-Laplacian feature. The QDA classifier trained with these top 5 features resulted in a 72.72% prediction accuracy on the test set.

CONCLUSION

Radiomic texture features extracted from the nodule on baseline CT scans were found to be predictive of response for NSCLC patients treated with immunotherapy. Multi-site validation is needed to establish the role of these features as predictive biomarker for response to immunotherapy in NSCLC patients.

CLINICAL RELEVANCE/APPLICATION

Our work suggests that we could better identify which patients are most likely to respond to and hence benefit from immunotherapy. From an economic perspective, identifying patients who are not likely to respond to immunotherapy could mean that expensive checkpoint inhibitor drugs would not be needlessly administered to these patients.

Part 2: Poster Presentations

Radiomic Features on Baseline Non-Contrast CT Predict Clinical Benefit for Pemetrexed Based Chemotherapy in Metastatic Lung Adenocarcinoma

Sagar Rakshit[1], Mahdi Orooji[2], Niha Beig[2], Mehdi Alilou[2], Nathan A. Pennell[1], James Stevenson[1], Marc A. Shapiro[1], Prabhakar Rajiah[3], Anant Madabhushi[2], Vamsidhar Velcheti[1]
[1]Cleveland Clinic Foundation, Cleveland, OH, USA [2]Case Western Reserve University, OH, USA, [3]University of Texas Southwestern Medical center, TX, USA

Introduction

Objective

To determine if computer extracted shape and texture features from within the nodule and the peritumoral zone on computerized tomographic (CT) scans can predict benefit and treatment response to pemetrexed based chemotherapy in pulmonary adenocarcinoma.

Background

- Pemetrexed based platinum doublet followed by maintenance pemetrexed for lung adenocarcinoma is the standard of care for patients with no actionable mutations. However many patients receiving such cytotoxic chemotherapy do not receive clinical benefit.
- Response rate to pemetrexed based regimens as initial treatment is around 24-31% while the disease control rate is around 60%[1-2].
- Currently there are no clinically validated biomarkers to identify patients who benefit from these treatments.

Related work and novel contribution

- Textural analysis to predict response to chemotherapy has been done predominantly on pre-treatment DCE-MRI and PET images[3-5].
- Ravanelli et al used pre-treatment CT images to predict response to first line chemotherapy in NSCLC [6].
- In this work we evaluate the predictive benefit of radiomic texture and shape features both within the peritumoral and tumoral compartments. Contributions are
  - Evaluate role of intra-tumoral texture and lesion shape in predicting response to Chemo.
  - Evaluate role of peritumoral morphology (via textural analysis) in predicting response to Chemo.
- Evaluate whether combination of intra-tumoral and peri-tumoral features is more predictive of Chemo response

Methodology

Step 1

Dataset curation: CT scans of patients who derived benefit and no benefit from pemetrexed based chemotherapy

Benefit: Objective response or >=12 cycles of pemetrexed

Step 2

- Annotation of ROI to delineate tumoral and peritumoral volume
- Peritumoral volume defined as the volume between tumor boundary and 7 pixels away. Distance heuristically determined.

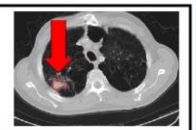

Step 3

- Extracting shape and texture feature from the intra and peritumoral compartment of annotated nodule from previous step
- 1108 radiomic descriptors were extracted

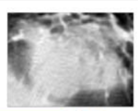

Experiment 1

Identify most predictive shape and texture features from the *intratumoral* compartment

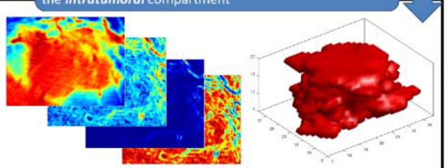

Experiment 2

Identify most predictive shape and texture features from the *peritumoral* compartment

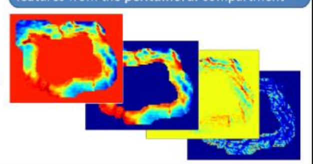

Experiment 3

Identify most predictive combination of *intratumoral and peritumoral* compartment

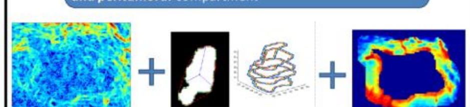

References

1. Scagliotti GV et al. Phase III Study Comparing Cisplatin Plus Gemcitabine With Cisplatin Plus Pemetrexed in Chemotherapy-Naive Patients With Advanced-Stage Non–Small-Cell Lung Cancer. J of Clinical Oncology.
2. Zinner RG et al. PRONOUNCE: randomized, open-label, phase III study of first-line pemetrexed + carboplatin followed by maintenance pemetrexed versus paclitaxel + carboplatin + bevacizumab followed by maintenance bevacizumab in patients ith advanced nonsquamous non-small-cell lung cancer. Journal of thoracic oncology
3. Ahmed A, Gibbs P, Pickles M, Turnbull L. Texture analysis in assessment and prediction of chemotherapy response in breast cancer. Journal of magnetic resonance imaging : JMRI. 2013;38(1):89-101
4. Michoux N, Van den Broeck S, Lacoste L, Fellah L, Galant C, Berlière M, et al. Texture analysis on MR images helps predicting non-response to NAC in breast cancer. BMC Cancer. 2015;15(1):1-13.
5. Tixier F et al. Intratumor heterogeneity characterized by textural features on baseline 18F-FDG PET images predicts response to concomitant radiochemotherapy in esophageal cancer. J of nuclear medicine
6. Ravanelli M et al. Texture analysis of advanced non-small cell lung cancer (NSCLC) on contrast-enhanced computed tomography: prediction of the response to the first-line chemotherapy. European radiology.

DoD Prostate Cancer Postdoctoral Training Award W81XWH-15-1-0613. National Cancer Institute of the National Institutes of Health R21CA167811-01, R21CA179327-01, R21CA195152-01, U24CA199374-01, the National Institute of Diabetes and Digestive and Kidney Diseases (R01DK098503-02], the DOD Prostate Cancer Synergistic Idea Development Award the DOD Lung Cancer Idea Development New Investigator Award , the DOD Prostate Cancer Idea Development Award; the CTSC Coulter Annual Pilot Grant, the VelaSano Grant from the Cleveland Clinic, the Case Comprehensive Cancer Center Pilot Grant, NSF I-Corps 2015, the Ohio Third Frontier Technology development Grant, the Wallace H. Coulter Foundation Program in the Department of Biomedical Engineering at Case Western Reserve University, Start up support through Department of Biomedical Engineering and Case Comprehensive Cancer Center at Case Western Reserve University.

Dataset

- Pre-treatment CT scans of N=65 patients treated with pemetrexed chemotherapy at Cleveland CLinic, 32 with and 33 without clinical benefit.
- Lesions were annotated by an expert reader on 3D slicer software

Method

- Feature selection strategy: Features are ranked based on the AUC values and Feed Forward feature selection.
- Linear Discriminant Analysis (LDA) classifier used for prediction. 4-fold cross validation was used for classifier optimization and evaluation.

Experimental results

- **Experiment 1:** Mean of Intratumoral sum average, the minimum of intratumoral Law L5xE5 and Sphericity are the most predictive radiomics, with AUC equals 69.5%, 67.2% and 64.1%, respectively. Figure 1 demonstrates the scatter plot of intratumoral features.
- **Experiment 2:** Mean of Peritumoral Law S5xW5 is the most informative texture feature with AUC=64%.
- **Experiment 3:** A combination of intratumoral and peritumoral radiomics achieve better prediction accuracy compared to either alone.
- Two of the top 3 ranked features were intratumoral, one was peritumoral. Figure 2 for the 3 features, AUC=0.78

Feature Category	Feature Vector	AUC
Intratumoral	Mean of Intratumoral Sum Average	69.5% ± 3.2%
	Minimum of Intratumoral Law L5xE5	67.2% ± 4.9%
	Sphericity	64.1% ± 3.7%
Peritumoral	Mean of Peritumoral Law S5xW5	64%±8.1%
Intratumoral+ Peritumoral	Mean of Intratumoral Sum Average+ Minimum of Intratumoral Law L5xE5+Mean of Peritumoral Law S5xW5	77.6% ± 1.9%

Table 1:Top performing radiomic features and AUC

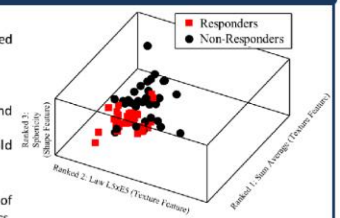

Figure 1: Scatter plot of the most informative intratumoral feature

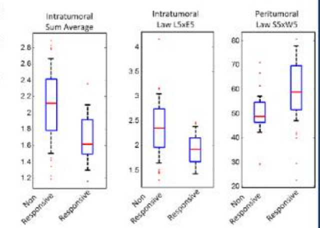

Figure 2: Box and whisker of the best radiomic features. (left) and (middle): Intratumoral texture and (right) Peritumoral texture

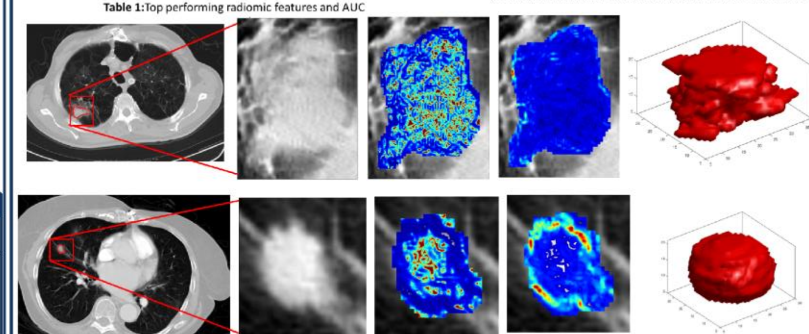

Figure 3: Qualitative demonstration of predictive intra- and peri- tumoral radiomics identified on: (Top Row) Non Responder and (Bottom Row) Responder. From left to right: Original CT, annotated nodule, Energy texture feature, Difference variance texture feature, sphericity shape feature

Concluding Remarks

- Our analysis highlights the impressive potential of non-invasive and cost-effective radiomics for precision medicine.
- To our knowledge this is the first study in lung cancer radiomics to correlate peritumoral features with response to chemotherapy.
- Combination of intra- and peri-tumoral features appears to better predict response to Chemo for NSCLC.
- Larger, multi-institutional cohort study is needed to validate the applicability of current findings.

Computerized Textural and Shape Analysis of Lung CT Enables Prediction of Extent of Tumor Infiltrating Lymphocytes (TIL) in Non-Small Cell Lung Cancer

Mahdi Orooji[1], Sagar Rakshit[2] ,Niha Beig[1], Mehdi Alilou[1], Nathan A. Pennell[2], James Stevenson[2], Marc A. Shapiro[2], Prabhakar Rajiah[3],Anant Madabhushi[1], Vamsidhar Velcheti[2]
[1]Case Western Reserve University, OH, USA, [2]Cleveland Clinic Foundation, Cleveland, OH, USA, [3]University of Texas Southwestern Medical center, TX, USA

Introduction

Objective

To determine if computer extracted shape and texture features of the nodule on computerized tomographic (CT) scans can be used in quantifying tumor infiltrating lymphocytes (TILs) in non-small cell lung cancer (NSCLC).

Background

- Tumor infiltrating lymphocytes are a part of the dynamic immune microenvironment of the tumor.
- Increased TILs have been consistently associated with better outcome in diverse human neoplasms, including melanoma, colorectal, triple- negative carcinomas and NSCLC[1].
- Clinical trials with immune checkpoint inhibitors report significant increase in TILs in responders on serial tumor biopsies[2,3].
- Radiomics refers to the comprehensive quantification of tumour phenotypes by using a large number of automatically extracted data-characterization algorithms [4].
- Monitoring TILs on treatment using radiomic features extracted from routine follow up computerized tomographic (CT) images can be a non-invasive surrogate to biopsy to detect early response.

Previous work and Novel Contribution

- Radiomic features have been previously correlated with tumor stage, tumor histology, tumor metabolism, survival, metastasis, response to chemoradiotherapy and the underlying gene expression profiles [4].
- To the best of our knowledge, first study evaluating shape and texture features on CT images to predict TIL extent

Methodology

Step 1: Identification of study population and annotation of CT images

- A cohort of 50 consecutive patients who underwent lobectomy at Cleveland Clinic for early stage NSCLC were identified and TIL were characterized using routine hematoxylin and eosin (H&E) slides.
- TILs on H&E surgical pathology specimens were quantified on a previously reported scale of 0 to 3 based on ratio of lymphocytes to tumor.
- Of the 50 cases 17 outliers who had high TILs (3+) or low TILs (0) were identified.
- Corresponding pre-surgical CT scans of the 17 outliers were anonymized and annotated on slicer-3D software to identify the tumor.
- The study team was provided with CT images from 4 patients with '0' TILs, 8 tumors with '3+' TILs and 5 tumors were blinded.

Step 2: Extraction of shape and texture features from annotated nodules

- Textural analysis was done on the entire tumor volume overcoming spatial heterogeneity in TILs.
- A total of 669 radiomic (textural and shape) features of the lung nodule were investigated.

Original CT Scan

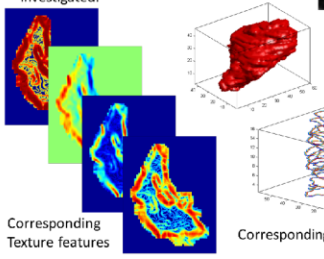

Corresponding Texture features

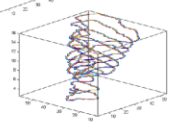

Corresponding shape features

Texture Features	Shape Features	
Haralick Features	Location	Convexity
Gray Features	Size	Equivalent Diameter
Gradient Features	Perimeter	Extension
Gabor Features	Eccentricity	Sphericity
LBP Feature	Compactness	
Law Features	Roughness	
Law Laplacian Features	Elongation	

Table 1: List of Radiomic categories used in study.

Step 3: Feature Selection and Classifier Modeling

- Features are ranked based the Fisher Criteria score. The top two informative texture features and the best shape feature is selected.
- The linear Discriminant Analysis (LDA) classifier divides the feature space into two subspaces, TIL positive an TIL negative

Experimental Design and Results

Experiment 1

Identifying the top radiomic features for distinguishing high from low TILs on CT

The Fisher Criteria feature ranking suggests that among texture features, "Standard deviation" and "Laws W5xW5" were ranked as the most discriminating. Sphericity was identified as most discriminating shape feature.

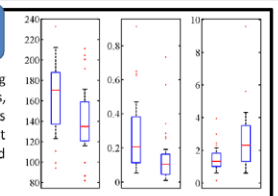

Figure 1: Box Whisker of most discriminative features. Left to right: mean of standard deviation, the mean of Law W5xW5, sphericity. In each box, the left bar is positive and right bar is negative.

Experiment 2

Evaluating machine learning classifier in distinguishing CT scans with different levels of TILs

- Linear Discriminant Analysis (LDA) classifier was applied to classify tumors as high or low TILs based on the mean of standard deviation and the mean of Law W5xW5 texture features and sphericity shape feature.
- Annotated CT images of 5 blinded cases were fed to LDA classifier previously trained with 12 number of cases.
- Out of 5 unknown cases, 4 of them classified correctly (Figure 2).

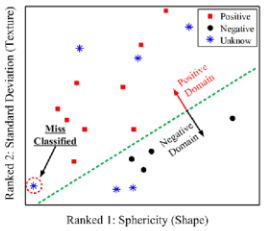

Figure 2 : Scatter plot shows the discriminability of the radiomics features in conjunction with a LDA classifier. Shown on the two axes are the, the mean of Standard deviation and Sphericity in discriminating high TILs (3+) versus low TILs (0).

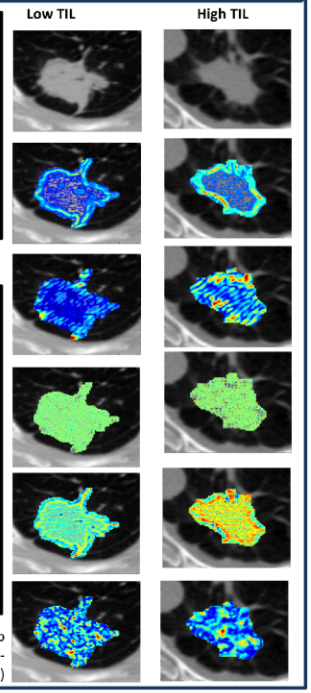

Figure 3: Qualitative demonstration of texture features of high and low TIL. From top to bottom: Original CT, Difference Variance, Gabor (π/4, √2/8), Law W5xW5, Law-Laplacian L5xL5, Gabor (5π/8, 1/2)

Concluding Remarks

- Preliminary proof of concept study suggesting that density of tumor infiltrating lymphocytes can be predicted by radiomic textural and shape analysis of non-contrast CT scans.
- In our current study, we correctly predicted the TIL quantification in 17 cases; 4 out of 5 blinded cases from the 17 studies.
- The current model was built on early stage lung cancer cases undergoing surgical resection for ease of TIL quantification. Further correlative work needs to be done in advanced NSCLC cases to increase applicability of protocol. Further validation with larger, multi-institutional cohorts is needed to improve the level of evidence of the preliminary results.

References

1. Tumeh PC, Harview CL, Yearley JH, Shintaku IP, Taylor EJM, Robert L, et al. PD-1 blockade induces responses by inhibiting adaptive immune resistance. Nature. 2014;515(7528):568-71
2. Herbst RS, Soria J-C, Kowanetz M, Fine GD, Hamid O, Gordon MS, et al. Predictive correlates of response to the anti-PD-L1 antibody MPDL3280A in cancer patients. Nature. 2014
3. Schalper KA, Brown J, Carvajal-Hausdorf D, McLaughlin J, Velcheti V, Syrigos KN, et al. Objective Measurement and Clinical Significance of TILs in Non–Small Cell Lung Cancer. JNCI Journal of the National Cancer Institute. Wu W, Parmar C, Grossmann P, Quackenbush J, Lambin P, Bussink J, et al. Exploratory Study to Identify Radiomics Classifiers for Lung Cancer Histology. Frontiers in Oncology. 2016;6
4. Yamazaki M, Ishikawa H, Kunli R, Tasaki A, Sato S, Ikeda Y, et al. A combination of preoperative CT findings and postoperative serum CEA levels improves recurrence prediction for stage I lung adenocarcinoma. European journal of radiology. 2015;84(1):178-84

DoD Prostate Cancer Postdoctoral Training Award W81XWH-15-1-0613. National Cancer Institute of the National Institutes of Health R21CA187811-01, R21CA179327-01, R21CA195152-01, U24CA199374-01, the National Institute of Diabetes and Digestive and Kidney Diseases (R01DK098503-02), the DOD Prostate Cancer Synergistic Idea Development Award the DOD Lung Cancer Idea Development New Investigator Award , the DOD Prostate Cancer Idea Development Award; the CTSC Coulter Annual Pilot Grant, the VelaSano Grant from the Cleveland Clinic, the Case Comprehensive Cancer Center Pilot Grant, NSF I-Corps 2015, the Ohio Third Frontier Technology development Grant, the Wallace H. Coulter Foundation Program in the Department of Biomedical Engineering at Case Western Reserve University, Start-up support through Department of Biomedical Engineering and Case Comprehensive Cancer Center at Case Western Reserve University.

A Combination of Radiomic Features From MRI and Ultrasound Appears to Better Predict Presence of Prostate Cancer: Validation Against Whole Mount Pathology

Mahdi Orooji [(1)]*, Mehdi Alilou[(1)], Rachel Sparks[(2)], Mirabela Rusu[(1)],B Nicolas Bloch[(3)], Ernest Feleppa[(4)], Dean Barratt[(2)], Lee Ponsky[(5)], Anant Madabhushi[(1)]**

(1) Center for Computation Imaging and Personalized Diagnostics (CCIPD), Cleveland, OH, USA, (2) Centre for Medical Image Computing, University College of London, London, UK
(3) Boston University School of Medicine, Boston, Massachusetts, USA, Lizzi Center for Biomedical Engineering, Riverside Research, USA, (4) University Hospital Case Medical Center, Case Western Reserve University, Cleveland, OH, USA,
*Mahdi.Orooji@case.edu, **Anant.Madabhushi@case.edu

CASE SCHOOL OF ENGINEERING
CASE WESTERN RESERVE UNIVERSITY
Center for Computational Imaging and Personalized Diagnostics

Introduction

Objective:

To evaluate whether the combination of computer extracted or radiomic image parameters from T2w MRI and Transrectal Ultrasound (TRUS) can better predict presence of prostate cancer compared to either modality individually.

Background:

- Multi-parametric MRI has shown promise in detecting, localizing, and grading prostate
- TRUS-guided biopsy is routine because TRUS is widely available and acquires real-time imagery. However, TRUS-guided biopsy has a low sensitivity, and initial biopsy misses approximately half of all men with prostate cancer.
- MRI-TRUS fusion, whereby MRI is acquired pre-operatively then aligned to TRUS during biopsy, allows for both modalities to be leveraged. MRI-TRUS fusion will enable the construction of joint classifiers, which leverage imaging characteristics on both MRI and TRUS, to detect, localize, and grade prostate cancer.

Related Work and Novel Contribution:

- Recently there has been a great deal of interest in developing computer aided diagnosis systems for identifying prostate cancer presence *in vivo* on MRI and ultrasound separately[1-3].
- Fully automated MRI-TRUS fusion, that spatially aligns MRI to TRUS via a probabilistic registration metric has been introduced in [4].
- No work we are aware of has attempted to address the issue of fusing computer derived features from MRI and ultrasound to create the best possible predictor of cancer *in vivo*.

Methodology

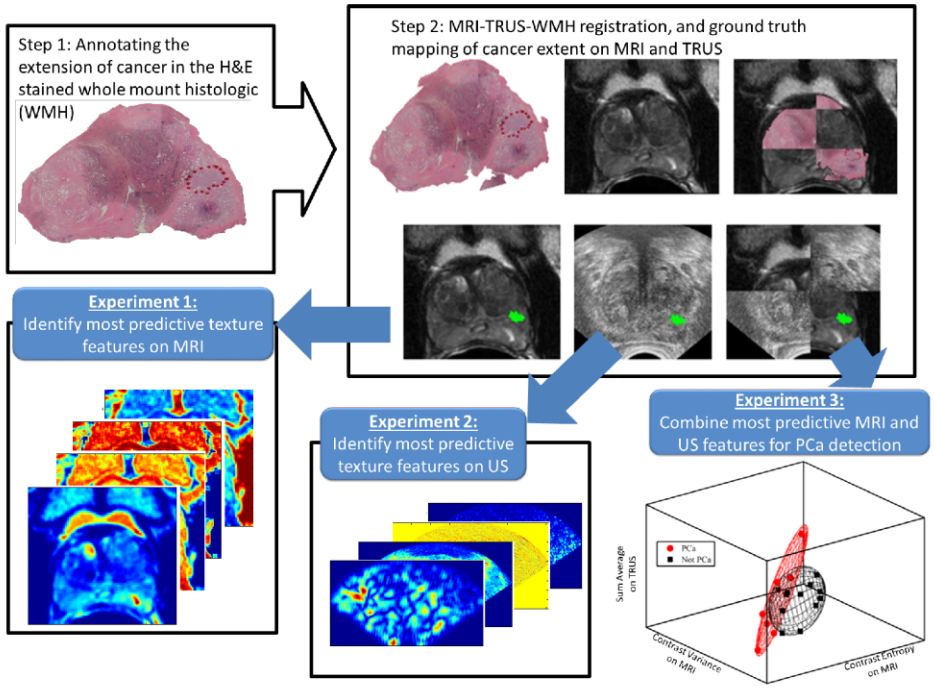

Experimental Design and Results

Dataset:

- 12 2D planar images obtained from the MRI and US scans of 3 patients, all of whom had biopsy confirmed prostate cancer and underwent radical prostatectomy.
- 3D B-mode ultrasound scan performed followed by a 3 Tesla MRI prior to surgery.
- Following surgery and histologic sectioning of the gland via a microtome, the H&E stained whole mount histologic (WMH) sections were digitized via a whole slide scanner and the regions of cancer annotated by an expert pathologist.

Experimental Results

- Experiment 1: Most predictive MRI feature "Contrast Variance", Best AUC = 83%.
- Experiment 2: Most predictive US feature "Sum Average", Best AUC = 78%
- Experiment 3: Combination of "Contrast Variance" and "Contrast Entropy" from MRI and "Sum Average" from US with a Fisher classifier yielded an AUC = 88%.
- The top 3 features for each modality and corresponding Fisher criteria values are shown in Figure 1.

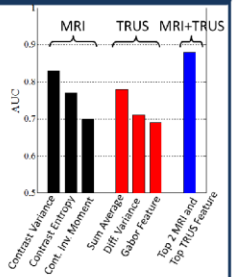

Figure 1: Bar plot of AUC values for the most informative texture features in MRI, TRUS, and the combination of them

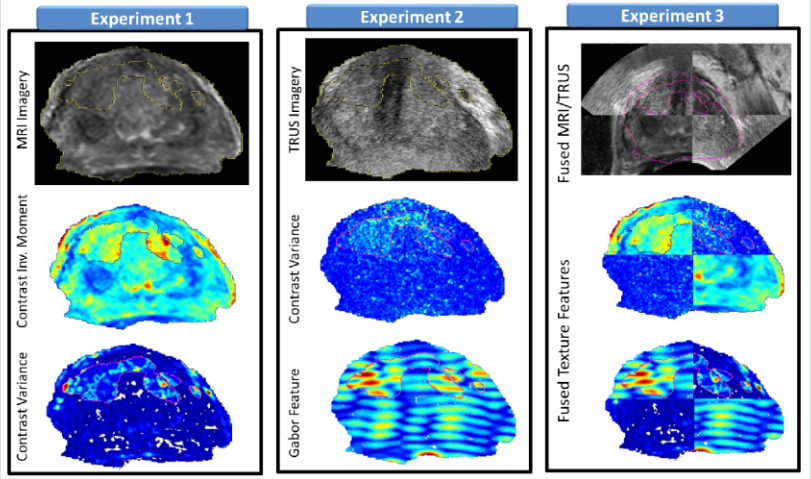

Figure 2: Top most predictive features identified on: (Left) MRI, (Middle) TRUS and (Right) Fusion of MRI/TRUS.

Concluding Remarks

We presented a framework to rank the performance of computer extracted MRI and ultrasound features in terms of their ability to identify prostate cancer. Our results in a small cohort suggests that we may be able to combine the MRI and ultrasound radiomic features to create a better classifier for prostate cancer detection compared to MRI or ultrasound alone.

Acknowledgments

DoD Prostate Cancer Postdoctoral Training Award W81XWH-14-PCRP-PTA, National Cancer Institute of the National Institutes of Health R21CA167811-01, R21CA179327-01, R21CA195152-01, U24CA199374-01, the National Institute of Diabetes and Digestive and Kidney Diseases (R01DK098503-02), the DOD Prostate Cancer Synergistic Idea Development Award the DOD Lung Cancer Idea Development New Investigator Award , the DOD Prostate Cancer Idea Development Award; the CTSC Coulter Annual Pilot Grant, the VelaSano Grant from the Cleveland Clinic, the Case Comprehensive Cancer Center Pilot Grant, NSF I-Corps 2015, the Ohio Third Frontier Technology development Grant, the Wallace H. Coulter Foundation Program in the Department of Biomedical Engineering at Case Western Reserve University, Start-up support through Department of Biomedical Engineering and Case Comprehensive Cancer Center at Case Western Reserve University.

References

[1]Emilie Niaf, Olivier Rouvière, Florence Mège-Lechevallier, Flavie Bratan, Carole Lartizien," Computer-aided diagnosis of prostate cancer in the peripheral zone using multiparametric MRI", Physics in Medicine and Biology 2011.
[2]Tiwari P, Kurhanewicz J, Rosen M, Madabhushi A. (2010) Semi supervised multi kernel (SeSMiK) graph embedding: Identifying aggressive prostate cancer via magnetic resonance imaging and spectroscopy. Med Image Comput Comput Assist Interv. 13(Pt 3):666-73
[3]Mehdi Moradi, Parvin Mousavi, Purang Abolmaesumi, Computer Aided Diagnosis of Prostate Cancer with Emphasis on Ultrasound-Based Approaches: A Review, Ultrasound in Medicine & Biology, Volume 33, Issue 7, July 2007, Pages 1010-1028, ISSN 0301-5629
[4]"Fully Automated Prostate Magnetic Resonance Imaging and Transrectal Ultrasound Fusion via a Probabilistic Registration Metric. Sparks R, Bloch BN, Feleppa E, Barratt D, Madabhushi A. Proc SPIE Int Soc Opt Eng. 2013 Mar 8;8671. doi: 10.1117/12.2007610.

Part 2: In Preparation Journal

Spatial Statistic Aware Segmentation Paradigm: Application on the Prostate Segmentation in the Transrectal Ultrasound Images

Mahdi Orooji[a,†],Mehdi Alilou[a] , Lee Ponsky[b], Anant Madabhushi[a,‡]
[†]mxo143@case.edu, [‡]axm788@case.edu
[a]Center for Computational Imaging and Personalized Diagnostics, Case Western Reserve University,
[b]University Hospital Case Medical Center, Case Western Reserve University

***Abstract*—Prostate needle biopsy guided by transrectal ultrasound (TRUS) is the current gold standard for prostate cancer (CaP) detection. An accurate detection of the prostate volume and boundary is influential on diagnosis, treatment, and follow up of CaP. Within this framework, prostate segmentation on TRUS imagery is performed via introduced spatial statistic aware segmentation paradigm. The spatial prior probability is calculated in the training phase, and is used to estimate the texture feature parameters corresponding to the prostate and the background. Estimated parameters is employed to represent an alternative probabilistic presentation of the prostate in TRUS. Results show the 3D prostate capsule is more pronounced in the new representation which ultimately results in more accurate segmentation. Modified active shape model (ASM) is introduced and applied in the new 3D TURS representation for prostate segmentation.**

***Index Terms*—Prostate Segmentation, Texture Feature Heatmap, Parameter Estimation, Expectation-Maximization, Maximum Likelihood Estimation, Active Shape Model**

I. Introduction

Prostate cancer (CaP) is the second-leading cause of cancer deaths in men and leading cause of cancer deaths men over age 50 in the United States. It is estimated 450,000 new CaP case swill be detected by 2015. Predictions also suggest one fourth of new CaP cases will be in men less than 65 years of age which emphasizes the necessity of early detection and localization of CaP. Prostate needle biopsy guided by transrectal ultrasound (TRUS) is the gold standard for CaP diagnosis. Determining the prostate volume and identifying the prostate capsule plays a crucial role in needle targeting. Due to the importance in delineating the prostate on TRUS, semi and fully automated prostate segmentation methods for TRUS imagery have been developed. Despite recent advances in transducer design, resulting in improved spatial and temporal resolution, TRUS image segmentation is still heavily influenced by the quality of data [1], [2]. Additionally, TRUS segmentation is vulnerable to variety of artifacts, such as, different levels of signal attenuation, shadowing artifacts, and speckle. Low contrast between areas of interest is another difficult problem in prostate segmentation on TRUS.

Previous prostate segmentation algorithms for TRUS image have focused on incorporating prior knowledge such as prostate shape [3] or prior spatial probability [4]. Recently, 2D or 3D boundary extraction methods have been developed based on probabilistic data association filters [2]. However, these approaches assume prior information for the prostate shape (such as concavity) and/or need manually placed initial seed locations inside the prostate [5]. Recently, active contour-based approaches have been used for prostate segmentation. These methods assumed prior spatial properties [6], or needs some initial points on [7] or near [8] the prostate boundary. These methods have also been employed to fuse multi-modal images of the prostate [9]. Our method is a fully automated semi-supervised segmentation algorithm that uses only the spatial prior probability for parameter estimation. Feature parameter estimation considers all voxels in an image; however, segmentation is performed on each voxel independently. Considering joint probability of extracted features and other criteria such as restricted maximum distance of voxels in the segments or morphology of the segments [10], the presented method can be generalized to exploit prior particular available knowledge.

In this work, we formulize a spatial statistic aware segmentation paradigm, and applied it for 3D segmentation of the prostate in the TRUS. Using introduced paradigm, a distribution parameters of 129 texture features in TRUS is estimated and the prostate/background probability heatmap is generated via using estimated distribution. A more informative alternative representation of the prostate in TRUS is introduced, and modified active shape model is applied on it for automatic annotation of the prostate boarder. The rest of the article is organized as follows. After the introduction in the first section, to increase the readability, in the second section the assumptions are described, the parameters are defined, and the problem of matter is formulized. The spatially aware distribution parameter estimation is elevated in the third section. Estimated distribution is employed in the forth section to introduce a new TRUS HeatMap Representation (THR). In section five, a modified adaptive active shape model is introduced and applied on THR. The performnce of the method is evaluated in section six and the paper is concluded in section seven.

II. Assumptions and Problem Formulation

As a problem statement, the goal is to segment the prostate in a TRUS image slide denoted by I. Note that, I is a 2D axial section of a 3D prostate gland. The 3D capsule

would be reconstructed by stacking the estimated prostate capsule. To increase the readability of the manuscript, we summarize the notation we used in the following. Here and subsequently, $\bar{a}$, $A_{Y\times X}$, $A^{\dagger}$, and $|A|$ imply a is a vector, A is a matrix with Y rows and X columns, a transpose of matrix A, and determinant of matrix A, respectively. Suppose N denotes the total number of voxels of I. By extracting L features from the original intensity image, we can reconstruct an observation matrix, $D_{N\times L} = [\bar{d}_1, \bar{d}_2, \cdots, \bar{d}_N]^{\dagger}$ where the vector $\bar{d}_n = \{d_{n,1}, d_{n,2}, \cdots, d_{n,L}\}$ for $n \in \{1, 2, \cdots, N\}$ is a feature vector corresponding to each voxel of I. To keep the generality of approach, I is desired to be segmented into K distinct sets of voxels, $S_1, \cdots, S_K$ such that the union of all segments cover the entire image, i.e., $\bigcup_{k=1}^{K} S_k = I$ and $\bigcap_{k=1}^{K} S_K = \emptyset$. The set of parameters of each segment that needs to be estimated is denoted by $\Theta = \{\mathcal{M}, \Lambda\}$ in which $\mathcal{M}_{K\times L} = [\bar{\mu}_1, \bar{\mu}_2, \cdots, \bar{\mu}_K]^{\dagger}$, for $\bar{\mu}_k = \{\mu_{k,1}, \mu_{k,2} \cdots, \mu_{k,L}\}$ is the mean of the kth segment. $\Lambda^2 = [\Sigma_1{}^2_{L\times L}, \Sigma_2{}^2_{L\times L}, \cdots, \Sigma_K{}^2_{L\times L}]$ is the set of covariance matrices of each segments where $\Sigma_k{}^2 = [\sigma^2_{i,j}]$. Table II lists the notations used throughout this paper.

A. Spatial Prior Probability

$\Xi_{N\times K} = [\xi_{n,k}]$, referred to as the *Spatial Prior Probability*, is the likelihood of the nth voxel belonging to kth segment, just based on its spatial information relative to the center of the ultrasound probe in an axial TRUS image. So, $\sum_{k=1}^{K} \xi_{n,k} = 1$, for any given n. Ξ is calculated from a set of J training studies, where for each study the prostate has been segmented by an expert. The origin for each study is set as the center of the TRUS probe, so that the location of voxels have a consistent position relative to the TRUS probe across all studies. $g_n^{(j)} = i$ for voxel n of jth training image belonging to class k where $k = 1$ represent prostate and $k = 0$ represent background. So, each element of the spatial prior probability matrix is calculated by averaging over all training images as:

$$\xi_{n,k} = \frac{1}{J} \sum_{j=1}^{J} g_n^{(k)} \tag{1}$$

Hence $\xi_{n,1}$ is the frequency of the nth voxel being located in the prostate across J training images.

The prostate is divided into three regions, the apex, the midgland and the base such that they have equal length in the sagittal axis. Two disjoint spatial prior probability was calculated corresponding to the region of interest, one for midgland and another one for the union of the apex and the base.

B. Feature Set Probability

$P_d(\bar{d}_n; \Theta)$ is the probability distribution function (PDF) of a set of features associated with voxel n, given the parameters (which are unknown). Without loss of generality, we assume $P_d(\bar{d}_n; \Theta)$ is modeled as a multivariate Gaussian distribution [4]. Note that even the intensity of the ultrasound image is Rayleigh distributed [11], [12]; however, considering the central limit theorem under weak dependence condition, the Gaussian distribution of the extracted texture features is a valid assumption [13].

Matrix of Segments: To make the feature set parameters estimation problem tractable, we define an auxiliary (latent) variable $Z_{N\times K} = [z_{n,k}]$, a *Matrix of Segments*, such that any arbitrary nth row of Z has only one element of 1 at kth column which implies nth voxel of I belongs to S_k, and the rest of the elements of the nth row are zero.

Parameter estimation is the solution of the following maximum likelihood equation:

$$\begin{aligned}\hat{\Theta} &= \arg\max_{\Theta} P(D|\Theta, \Xi) \\ &= \arg\max_{\Theta} \sum_{Z} \log\Big(P(D|Z, \Theta, \Xi) P(Z|\Theta, \Xi)\Big). \end{aligned} \tag{2}$$

The conditional distribution of the observation matrix given Θ and Z is given by:

$$P(D|Z, \Theta, \Xi) = \prod_{n=1}^{N} P(\bar{d}_n|Z, \Theta) = \tag{3}$$

$$\prod_{n=1}^{N} \prod_{k=1}^{K} \left[\frac{1}{(2\pi)^{L/2}|\Sigma_k|} \exp\Big((\bar{d}_n - \bar{\mu}_k)^{\dagger} \Sigma_k^{-2} (\bar{d}_n - \bar{\mu}_k)\Big)\right]^{z_{n,k}}$$

The matrix of segments is independent of the distribution parameters and its probability value is a function of spatial prior probability matrix as follows:

$$P(Z|\Theta, \Xi) = P(Z|\Xi) = \prod_{n=1}^{N} \prod_{k=1}^{K} [\xi_{n,k}]^{z_{n,k}} \tag{4}$$

One should note that for other feature distributions rather than Gaussian (such as the distribution of the intensity in TRUS images which is Rayleigh distribution [11], [12]), (3) needs to be substituted by a proper corresponding distribution function.

III. Spatial Aware Distribution Parameter Estimation

It is assumed that the TRUS image is consist of two segments, the prostate and the background. Constrained to the calculated prior spatial probability in (1), we employed an iterative expectation-maximization algorithm to estimate the parameters associated with the prostate and the background in the TRUS for each individual texture feature. In the other words, for a given observation matrix D, we estimate the matrix of parameters, $\{\mathcal{M}, \Lambda^2\}$. Using the estimated parameters, we introduced a new representation of the TRUS in section IV.

It is guaranteed that the expectation-maximization algorithm converges to the local maximum likelihood, however, the convergence of it to the global maximum and the legitimacy of the results is very reliant on the initialization [14].

To improve the parameter estimation, we introduced parameter estimation method, namely Decoupled Maximum Likelihood (DML), that employed the spatial prior probability for a sub-optimum maximum likelihood estimation. The sub-optimum estimated parameters are used an initial estimation of the parameters in the expectation-maximization algorithm. Our assessments shows the introduced method converges to

TABLE I
DESCRIPTION OF NOTATION USED THROUGHOUT THIS PAPER.

Notation	Description	Notation	Description
I	TRUS image scene.	$\Theta = \{\mathcal{M}, \Lambda\}$	Set of actual parameters.
N	Total number of pixels.	$\hat{\Theta} = \{\hat{\mathcal{M}}, \hat{\Lambda}\}$	Set of estimated parameters.
L	Total number of extracted features.	$\bar{\mu}_k = [\mu_{k,l}]_{1\times L}$	Vector of actual means of kth segment.
K	Assumed number of segments.	$\hat{\bar{\mu}}_k = [\hat{\mu}_{k,l}]_{1\times L}$	Vector of estimated means of kth segment.
$D_{N\times L}$	Matrix of observations.	$\Sigma_k^2 = [\sigma^2_{k_{i,j}}]_{L\times L}$	Set of actual covariance matrix of kth segment.
$\bar{d}_n$	Features vector of nth voxel.	$\hat{\Sigma}_k^2 = [\hat{\sigma}^2_{k_{i,j}}]_{L\times L}$	Set of estimated covariance matrix of kth segment..
$\Xi = [\xi_{n,k}]_{N\times K}$	Spatial prior probability matrix.	$I_f(\theta)$	Fisher Information of parameter θ.

the global maximum with less number of the iterations and does not trap on the local maximum.

A. Decoupled Maximum Likelihood (DML) Approach for Initial Estimation of the Parameters

By substituting corresponding values from (3) and (4) into (2), one can note that the maximum likelihood problem does not have an analytical closed form solution. When the analytical solution does not exist, generalized maximum likelihood ratio test (GLRT) is proposed [15]. GLRT is not an optimum solution, because instead of maximizing the likelihood ratio, independently treats the nominator and the denominators of the likelihood ratio and maximize them separately [16]. So, it results in the sub-optimum answer. Using GLRT algorithm, we introduced the decoupled maximum likelihood to estimate the parameters of the nominator (corresponding to the prostate) and the denominator (corresponding to the background) separately. The algorithm is as follows.

The parameters of kth segment is denoted by $\theta_k \triangleq \{\bar{\mu_k}, \Sigma_k^2\}$ for $k = 1$ and 2 corresponding to the background and the prostate, respectively. $\hat{\theta}_k^{(\mathrm{DML})}$ are estimated parameters of kth segment obtained by and decoupled maximum likelihood approach. So,

$$\hat{\theta}_k^{(\mathrm{DML})} = \arg\max_{\theta_k} \; P(D|\theta_k, \Xi), \text{ for } 1 \le k \le K \tag{5}$$

From (5), it is implied that the parameter estimation problem for each segment is decoupled to become tractable. To solve (5) we have,

$$P(D|\theta_k, \Xi) \tag{6}$$
$$= \prod_{n=1}^{N} \left[\frac{1}{(2\pi)^L |\Sigma_k|} \exp\left((\bar{d}_n - \bar{\mu}_k)^\dagger \Sigma_k^{-2} (\bar{d}_n - \bar{\mu}_k) \right) \right]^{\xi_{n,k}}$$

After some manipulation one can show that the solution of DML parameter estimation from (6) is given by:

$$\frac{\partial}{\partial \bar{\mu_k}} P(D|\theta_k, \Xi) = 0 \Longrightarrow \quad \hat{\bar{\mu}_k} = \frac{\sum_{n=1}^{N} \xi_{n,k} \bar{d}_n}{\sum_{n=1}^{N} \xi_{n,k}} \tag{7}$$

$$\frac{\partial}{\partial \Sigma_k^2} P(D|\theta_k, \Xi) = 0 \Longrightarrow \quad \hat{\Sigma_k^2} = \frac{\sum_{n=1}^{N} \xi_{n,k} (\bar{d}_n - \hat{\bar{\mu}_k})^2}{\sum_{n=1}^{N} \xi_{n,k}} \tag{8}$$

The estimated mean and variance from (7) and (8) are employed as an initial mean and variance in the next step.

B. Parameters Estimation Per Individual Texture Feature

The solution of the Maximum Likelihood (ML) Ratio Test for each texture feature is the optimum unsupervised parameter estimation approach [15], [17]. However, ML is too complicated to be derived analytically. Hence, we employ an iterative algorithm, inspired by the Expectation-Maximization (EM) mixture model parameter estimation approach, to estimate values of Θ. EM is a powerful iterative algorithm to estimate the parameters of the mixture models when the associated log-likelihood maximization problem is too complicated to solve analytically. Using the same approach, we modified the two steps of Expectation and Maximization as follows:

Expectation Step:: Current and revised estimation of Θ are denoted by Θ^{OLD} and Θ^{NEW}, respectively. The conditional expectation of $\log P(D, Z|\Theta)$ given D and the current estimation of Θ is given by,

$$\mathcal{Q}(\Theta; \Theta^{\mathrm{OLD}}) = E_Z \left[\log P(D, Z|\Theta) \right] \tag{9}$$
$$= \sum_{n=1}^{N} \sum_{k=1}^{K} E_Z \left[z_{n,k} \middle| D, \Theta^{\mathrm{OLD}} \right] \times$$
$$\left(\log \xi_{n,k} - \frac{L}{2} \log 2\pi - \log |\Sigma| + (\bar{d}_n - \bar{\mu}_k)^\dagger \Sigma_k^{-2} (\bar{d}_n - \bar{\mu}_k) \right)$$

where $E_z[.|x]$ is the conditional expectation given x, respect to z. After some manipulation one can show that:

$$\gamma_{n,k} \triangleq E_Z \left[z_{n,k} \;\middle|\; D, \Theta^{\mathrm{OLD}} \right] \tag{10}$$
$$= \frac{\xi_{n,k} P\left(\bar{d}_n \;\middle|\; z_{n,k}, \Theta^{\mathrm{OLD}} \right)}{\sum_{k=1}^{K} \xi_{n,k} P\left(\bar{d}_n \;\middle|\; z_{n,k}, \Theta^{\mathrm{OLD}} \right)}$$

Maximization Step:: It has been shown in [18] that the log-likelihood function is the monotone increasing function of the number of EM iteration steps. So, regardless of the initial value of Θ, EM converges. Θ^{NEW}, the new values of parameters, are the solution of:

$$\Theta^{\mathrm{NEW}} = \arg\max_{\Theta} \mathcal{Q}\left(\Theta, \Theta^{\mathrm{OLD}}\right) \tag{11}$$

By calculating the partial derivative of (9) and (10) respect to $\bar{\mu}_k$ and Σ_k, one can show that

$$\hat{\mu}_{k,l} = \frac{\sum_{n=1}^{N} \gamma_{n,k} d_{n,l}}{\sum_{n=1}^{N} \gamma_{n,k}}, \tag{12}$$

$$\hat{\sigma}^2_{k,l} = \frac{\sum_{n=1}^{N} \gamma_{n,k} (d_{n,l} - \mu_{k,l})^2}{\sum_{n=1}^{N} \gamma_{n,k}} \tag{13}$$

IV. TRSU HeatMap Representation (THR)

Prostate segmentation in TRUS is a challenging task mainly due to the high inherent noise of the ultrasound images [19]. On the other side, the proficiency of the texture features in the prostate segmentation is already investigated [20]. We employed the power of the texture features in presenting the prostate in the ultrasound images and also the spatial statistics information to introduce an alternative representation of the TRUS image, in which the prostate capsule is more pronounced in compare to the original TRUS image. We named it the *TRUS-HeatMap Representation (THR)* .

To generate the THM representation, we need to generate the heatmap probability of the foreground and the background per feature. To do so, the first step is calculating the spatial prior probability by substituting the prostate capsule annotations in (1). Because the size of the prostate capsule in the apex and the base are close and it is relatively smaller than the size of the prostate in the midgland [21], so, we generated two disjoint spatial prior probability model for two sets of the apex/based and midgland.

In the second step texture features were extracted for a given TRUS image. In this articled we employed total of 129 texture features which described in Table II. Considering the spatial prior probability, in the third step we employed the Spatiall Aware Distribution Parameter Estimation Method introduced in section III to answer which segments in conjunction with which set of parameters are going to maximize the likelihood of observed extracted texture features of a TRUS image. To improve the proficiency of EM-based parameter estimation method, as it was described in the subsection III-A, we included the Decoupled Maximum Likelihood approach for initial estimation of the parameters in the third step.

And finally in the fourth step, the estimated distribution parameters corresponding to the foreground and the background for each feature is used to generate the foreground and the background probability heatmap. Figure 1 demonstrates the heatmap generation schematic for a texture feature. Figure 2 demonstrates the heatmap of the prostate and the background for Haralick features [22].

A. Adaptive Combination of the Texture Feature's Heatmaps to Generate THR

After calculating the probability heatmap of the foreground and the background for each feature, we need to find which feature in the foreground and which feature in the background has the highest capability of the prostate segmentation. To do so, we need to define a proficiency metric for foreground heatmaps and the background heatmaps.

$$\phi_{\text{Pr}} \triangleq \frac{\sum_{\forall n} z_{n,1} f^{pr}(d_n)}{\sum_{\forall n} z_{n,1}} \tag{14}$$

$$\phi_{\text{Bk}} \triangleq \frac{\sum_{\forall n} z_{n,0} \left(1 - f^{pr}(d_n)\right)}{\sum_{\forall n} z_{n,0}} \tag{15}$$

By combining the estimated probability of the prostate and the estimated probability of the background, we generated the prostate probability heat-map. Defined proficiency metric is employed to find the most proficient texture features for discriminating the prostate from the background. So, we added the proficiency weighted heatmaps to obtain the final prostate heatmap. Finally, AAM is applied on the prostate probability heatmap from the previous step for prostate segmentation in TRUS. Figure 3 demonstrates the prostate heatmap.

B. Calculating the Heat-map

Estimated features parameters, $\hat{\Theta}$, induce maximum likelihood image segmentation regardless of the parameter estimation approach (DML or ML). The prostate heat-map is defined as the conditional probability (given estimated parameters) that a voxel n belongs to the prostate which would be:

$$P(z_{n,1} = 1 | \hat{\Theta}) \tag{16}$$
$$= \frac{1}{\mathfrak{P}} \left[\xi_{n,1} P\left(\bar{d}_n | \hat{\bar{\mu}}_1, \hat{\Sigma}^2_1\right) + \xi_{n,0} \left(1 - P\left(\bar{d}_n | \hat{\bar{\mu}}_0, \hat{\Sigma}^2_0\right)\right)\right]$$

where $\mathfrak{P}$ is a normalization factor to guarantee that the heatmap values are in the range of 0 to 1.

V. Adaptive Active Shape Model on TRUS HeatMap

VI. Experimental Results

A. Dataset

The presented EM-based segmentation method was applied on 3D Transrectal Ultrasound (TRUS) images for six patients. TRUS images was acquired using a bi-planer side-firing transrectal probe. A prostate boundary on TRUS was manually delineated by an expert radiologist. To correct for the possible TRUS attenuation artifacts (due to the fact that pixels closer to the probe appear brighter), we employed the method in [4].

References

[1] S. Ghose, J. Mitra, A. Oliver, R. Mart, X. Llad, J. Freixenet, J. Vilanova, J. Comet, D. Sidib, and F. Meriaudeau, "Advanced concepts for intelligent vision systems," ser. Lecture Notes in Computer Science, J. Blanc-Talon, W. Philips, D. Popescu, P. Scheunders, and P. Zemk, Eds. Springer Berlin Heidelberg, 2012, vol. 7517, pp. 190–200. [Online]. Available: http://dx.doi.org/10.1007/978-3-642-33140-4_17

[2] R. M. X. L. J. C. V. J. F. J. M. D. S. F. M. Soumya Ghose, Arnau Oliver, "A survey of prostate segmentation methodologies in ultrasound, magnetic resonance and computed tomography images," *Computer Methods and Programs in Biomedicine*, vol. 108, no. 1, pp. pp. 262–287, 2012.

[3] W. Qiu, J. Yuan, E. Ukwatta, D. Tessier, and A. Fenster, "Three-dimensional prostate segmentation using level set with shape constraint based on rotational slices for 3d end-firing trus guided biopsy," *Medical Image Computing and Computer-Assisted Intervention MICCAI 2012*, vol. 1, 2012.

[4] R. Sparks and et al., "Fully automated prostate magnetic resonance imaging and transrectal ultrasound fusion via a probabilistic registration metric," in *Proceedings of the SPIE*, vol. 8671, 2013.

TABLE II
DESCRIPTION OF THE TEXTURE FEATURES USED FOR PROSTATE SEGMENTATION IN TRUS.

Feature category	Descriptor	Intuitive Description
Haralick features (Repeated occurrence of grey level configuration in the texture represented via the grey-level co-occurrence matrix (GLCM), which varies rapidly with distance in fine textures and slowly in large textures)	Inverse Difference Moment (IDM)	IDM is a reflection of the presence or absence of uniformity, and hence is a measure of local regions of homogeneity High IDM: Higher presence of locally uniform windows in GLCM Low IDM: Higher presence of locally heterogeneous windows in GLCM
	Correlation	Quantifies the linear patterns in an image based on the distance parameter.
	Sum Entropy	Measure of GLCM relationship to distribution of intensity with respect to entropy. Entropy is the measure of disorder.
	Sum Variance	Measure of GLCM relationship to distribution of intensity with respect to variance High sum variance: greater standard deviation of sum average Low sum variance: low standard deviation of sum average
Laws features	E5, L5, S5	Combining E- Edges, L- Level and S- Spots in both X any Y directions
Laplacian pyramids		Multi-resolution filters capture edges at different levels
Gray level features		The basic, intensity based features including mean, median, range and standard deviation.
Gabor Features		Oriented textures via changes in direction and scale; capture microarchitectures
Gradient Features		Represent the directional change in the intensity values of pixels in the ROI
Local Binary Pattern		Thresolding the window with the center pixel value.

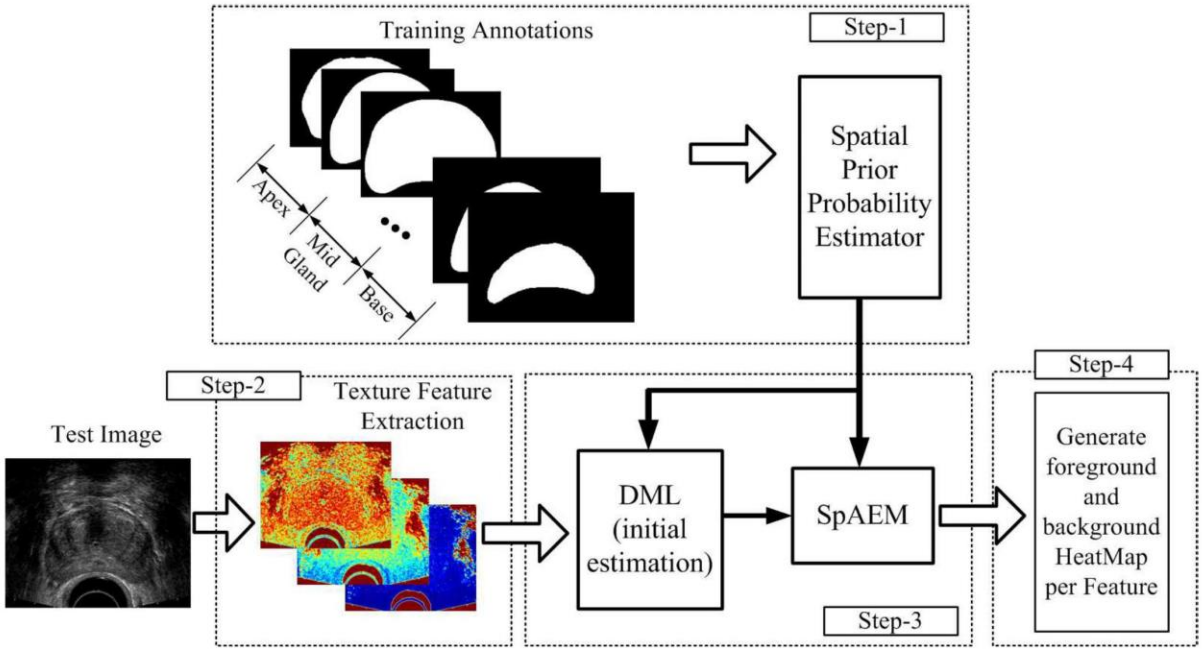

Fig. 1. Schematic of four steps used for generating the foreground and background heat-map per texture feature.

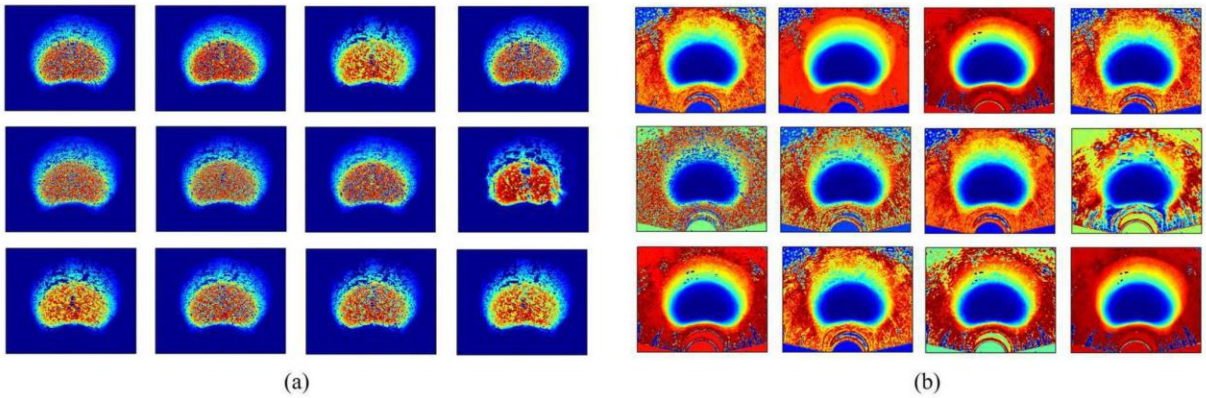

(a) (b)

Fig. 2. The probability heatmap of (a) the foreground probability and (b) the background probability.

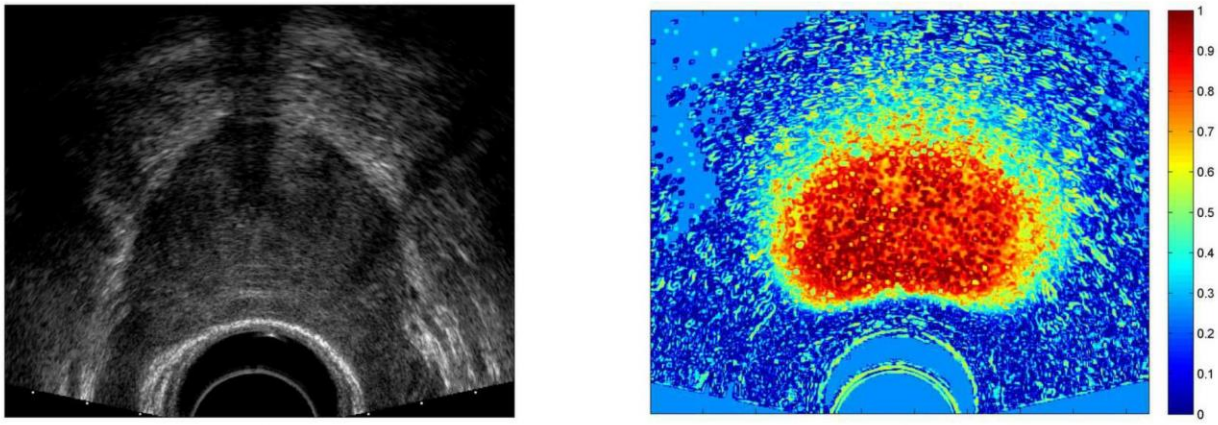

(a) (b)

Fig. 3. (a) TRUS images of a prostate and (b) corresponding the prostate heatmap.

[5] P. Abolmaesumi and at al, "An interacting multiple model probabilistic data association filter for cavity boundary extraction from ultrasound images," *Medical Imaging, IEEE Transactions on*, vol. 23, no. 6, pp. 772–784, 2004.

[6] J. Xu, J. P. Monaco, and A. Madabhushi, "Markov random field driven region-based active contour model (maracel): application to medical image segmentation," in *Proceedings of the 13th international conference on Medical image computing and computer-assisted intervention: Part III*, ser. MICCAI'10. Berlin, Heidelberg: Springer-Verlag, 2010, pp. 197–204. [Online]. Available: http://dl.acm.org/citation.cfm?id=1926877.1926903

[7] J. Yezzi, A., S. Kichenassamy, A. Kumar, P. Olver, and A. Tannenbaum, "A geometric snake model for segmentation of medical imagery," *Medical Imaging, IEEE Transactions on*, vol. 16, no. 2, pp. 199–209, 1997.

[8] Y. Yu, J. A. Molloy, and S. Acton, "Segmentation of the prostate from suprapubic ultrasound images," *Medical Physics*, vol. 1, 2004.

[9] S. S. Mahdavi, , and et al., "Fusion of ultrasound b-mode and vibro-elastography images for automatic 3-d segmentation of the prostate," *Medical Imaging, IEEE Transactions on*, vol. 31, no. 11, pp. 2073–2082, 2012.

[10] C. Carson and et al., "Blobworld: image segmentation using expectation-maximization and its application to image querying," *Pattern Analysis and Machine Intelligence, IEEE Transactions on*, vol. 24, no. 8, pp. 1026–1038, 2002.

[11] J. Goodman, *Speckle Phenomena in Optics: Theory and Applications*. Roberts & Company, 2007. [Online]. Available: http://books.google.com/books?id=TynXEcS0DncC

[12] A. Sarti, C. Corsi, E. Mazzini, and C. Lamberti, "Maximum likelihood segmentation of ultrasound images with rayleigh distribution," *Ultrasonics, Ferroelectrics, and Frequency Control, IEEE Transactions on*, vol. 52, no. 6, pp. 947–960, June 2005.

[13] B. Rosen, "On the central limit theorem for sums of dependent random variables," *Zeitschrift fr Wahrscheinlichkeitstheorie und Verwandte Gebiete*, vol. 7, no. 1, pp. 48–82, 1967.

[14] C. F. J. Wu, "On the convergence properties of the em algorithm," *The Annals of Statistics*, vol. 11, no. 1, pp. pp. 95–103, 1983.

[15] H. L. V. Trees, *Detection, Estimation, and Modulation Theory: Radar-Sonar Signal Processing and Gaussian Signals in Noise*. Melbourne, FL, USA: Krieger Publishing Co., Inc., 1992.

[16] O. Zeitouni, J. Ziv, and N. Merhav, "When is the generalized likelihood ratio test optimal?" *Information Theory, IEEE Transactions on*, vol. 38, no. 5, pp. 1597–1602, 1992.

[17] J. Neyman and E. S. Pearson, "On the use and interpretation of certain test criteria for purposes of statistical inference: Part i," *Biometrika*, vol. 20A, no. 1/2, pp. pp. 175–240, 1928. [Online]. Available: http://www.jstor.org/stable/2331945

[18] C. M. Bishop, *Pattern Recognition and Machine Learning (Information Science and Statistics)*. Secaucus, NJ, USA: Springer-Verlag New York, Inc., 2013.

[19] O. Michailovich and A. Tannenbaum, "Despeckling of medical ultrasound images," *Ultrasonics, Ferroelectrics, and Frequency Control, IEEE Transactions on*, vol. 53, no. 1, pp. 64–78, Jan 2006.

[20] Y. Zhan and D. Shen, "Deformable segmentation of 3-d ultrasound prostate images using statistical texture matching method," *Medical*

Part 3: Proof of Registration

Mahdi Orooji <mxo143@case.edu>

Registration Confirmation and Receipt #937388
1 message

ASCO Annual Meeting Registration <ascoregistration@spargoinc.com> Thu, Jun 2, 2016 at 7:17 PM
To: mxo143@case.edu

ASCO ANNUAL MEETING
COLLECTIVE WISDOM

REGISTRATION CONFIRMATION
June 3-7, 2016
Pre-Annual Meeting Educational Programs: June 2-3
Exhibits: June 4-6
McCormick Place | Chicago, Illinois

Please use this bar code, in print or on your phone, onsite in order to print your badge!

View it on your Phone

Registration Confirmation and Receipt #937388
ASCO Annual Meeting
June 03 - June 7, 2016
McCormick place
Chicago, IL

Registration Confirmation Number/Badge ID: 937388
Date of Registration: 06/02/2016
Registration Type: Attendee
Name: Mahdi Orooji, PhD
Company: Case Western Reserve University
Address: 523 Wickenden Building, 10900 Euclid Ave
Address 2: case western reserve university
City/State/Zip: Cleveland, OH 44106
Country: USA
Phone: 2256109702
Mobile Phone: (225) 610-9702
Email: mxo143@case.edu

Cancellations/Changes

Select here for registration changes and information

Hotel Information

Select here for hotel reservations and information

Travel Information

Select here for travel and ground transportation information

Keep Up With the Latest

Thank you for registering for the 2016 ASCO Annual Meeting to be held at McCormick Place in Chicago, Illinois. Please take a moment to review the information in this confirmation to confirm that it is correct. This is both your confirmation and your receipt. Please print and retain this document for your records.

REGISTRATION
Annual Meeting Registration with Virtual Meeting
$170.00

Mahdi Orooji <mxo143@case.edu>

RSNA 2016 Confirmation {RSN161:78397}

1 message

RSNA Customer Service <email_confirm@confmail.experient-inc.com> Thu, Nov 24, 2016 at 2:33 AM
To: mahdi.orooji@case.edu

***** Please do not reply to this e-mail. It was sent from an automated system. *****

Confirmation

Congratulations! You have successfully registered for RSNA 2016, our 102nd Scientific Assembly and Annual Meeting, November 27 - December 2, at McCormick Place, Chicago.

View the full meeting program and build your RSNA 2016 agenda at *Meeting.RSNA.org*.

Badges will be mailed in early November to all full conference attendees enrolled by October 1. After October 1, badges will be available for pickup at McCormick Place.

Registration Locations:

- South Building – Level 1
- Lakeside Center East – Level 2
- North Building – Level 2

Questions? Email *RSNA@experient-inc.com*.

Access Registration

Add To Calendar

Profile

Registrant ID: 78397
Mahdi Orooji
Ctr For Computational Imaging & Personalized Diagnostics
10900 Euclid Ave
Cleveland, OH 44106 USA

Part 4: US Patent

US 20160155225A1

(19) **United States**

(12) **Patent Application Publication**

Madabhushi et al.

(10) **Pub. No.: US 2016/0155225 A1**

(43) **Pub. Date: Jun. 2, 2016**

(54) **TEXTURAL ANALYSIS OF LUNG NODULES**

(71) Applicant: **Case Western Reserve University**, Cleveland, OH (US)

(72) Inventors: **Anant Madabhushi**, Shaker Heights, OH (US); **Mirabela Rusu**, Cleveland, OH (US); **Mahdi Orooji**, Cleveland, OH (US); **Mehdi Alilou**, Cleveland, OH (US)

(21) Appl. No.: **14/873,611**

(22) Filed: **Oct. 2, 2015**

Related U.S. Application Data

(60) Provisional application No. 62/085,616, filed on Nov. 30, 2014.

Publication Classification

(51) **Int. Cl.**

G06T 7/00	(2006.01)
A61B 6/03	(2006.01)
A61B 6/00	(2006.01)
G06T 7/40	(2006.01)

(52) **U.S. Cl.**

CPC ***G06T 7/0012*** (2013.01); ***G06T 7/0081*** (2013.01); ***G06T 7/40*** (2013.01); ***A61B 6/032*** (2013.01); ***A61B 6/50*** (2013.01); *G06T 2207/10081* (2013.01); *G06T 2207/30064* (2013.01); *G06T 2207/30096* (2013.01)

(57) **ABSTRACT**

Methods, apparatus, and other embodiments associated with classifying a region of tissue using textural analysis are described. One example apparatus includes an image acquisition logic that acquires an image of a region of tissue demonstrating GGO nodule pathology, a delineation logic that distinguishes GGO nodule tissue within the image from the background of the image, a texture logic that extracts a set of texture features from the image, a phenotype signature logic that computes a phenotypic signature from the image, a shape logic that extracts a set of shape features from the image, and a classification logic that classifies the GGO nodule tissue based, at least in part, on the set of texture features, the phenotypic signature, or the set of shape features. A prognosis for a patient may be provided based on the classification of the image.

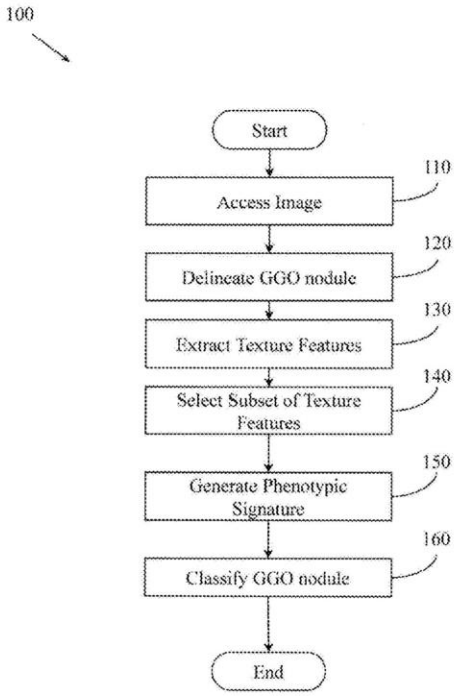

US 20170035381A1

(19) **United States**

(12) **Patent Application Publication**

(10) **Pub. No.: US 2017/0035381 A1**

(43) **Pub. Date: Feb. 9, 2017**

Madabhushi et al.

(54) **CHARACTERIZING DISEASE AND TREATMENT RESPONSE WITH QUANTITATIVE VESSEL TORTUOSITY RADIOMICS**

(71) Applicant: **Case Western Reserve University**, Cleveland, OH (US)

(72) Inventors: **Anant Madabhushi**, Shaker Heights, OH (US); **Mahdi Orooji**, Cleveland, OH (US); **Mirabela Rusu**, Cleveland, OH (US); **Philip Linden**, Pepper Pike, OH (US); **Robert Gilkeson**, Cleveland Heights, OH (US); **Nathaniel Mason Braman**, Cleveland, OH (US)

(21) Appl. No.: **15/226,148**

(22) Filed: **Aug. 2, 2016**

Related U.S. Application Data

(60) Provisional application No. 62/201,837, filed on Aug. 6, 2015.

Publication Classification

(51) **Int. Cl.**

A61B 6/00	(2006.01)
G06T 11/00	(2006.01)
A61B 5/08	(2006.01)
G06K 9/00	(2006.01)
A61B 6/03	(2006.01)
G06T 7/00	(2006.01)
G06K 9/46	(2006.01)

(52) **U.S. Cl.**

CPC ***A61B 6/5217*** (2013.01); ***G06T 7/0081*** (2013.01); ***G06T 11/003*** (2013.01); ***G06K 9/4604*** (2013.01); ***G06K 9/00147*** (2013.01); ***A61B 6/032*** (2013.01); ***A61B 5/08*** (2013.01); *G06T 2207/10081* (2013.01); *G06T 2207/20081* (2013.01); *G06T 2207/20141* (2013.01); *G06T 2207/30101* (2013.01); *G06T 2207/30064* (2013.01); *A61B 2034/105* (2016.02)

(57) **ABSTRACT**

Methods, apparatus, and other embodiments associated with classifying a region of tissue using quantified vessel tortuosity are described. One example apparatus includes an image acquisition logic that acquires an image of a region of tissue demonstrating cancerous pathology, a delineation logic that distinguishes nodule tissue within the image from the background of the image, a perinodular zone logic that defines a perinodular zone based on the nodule, a feature extraction logic that extracts a set of features from the image including a set of tortuosity features, a probability logic that computes a probability that the nodule is benign, and a classification logic that classifies the nodule tissue based, at least in part, on the set of features or the probability. A prognosis or treatment plan may be provided based on the classification of the image.

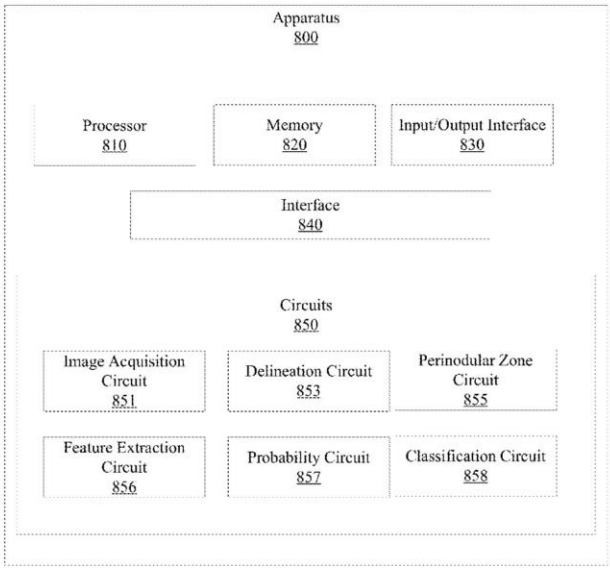

US 20170039737A1

(19) **United States**

(12) **Patent Application Publication** (10) **Pub. No.: US 2017/0039737 A1**

Madabhushi et al. (43) **Pub. Date: Feb. 9, 2017**

(54) **DECISION SUPPORT FOR DISEASE CHARACTERIZATION AND TREATMENT RESPONSE WITH DISEASE AND PERI-DISEASE RADIOMICS**

(71) Applicant: **Case Western Reserve University**, Cleveland, OH (US)

(72) Inventors: **Anant Madabhushi**, Shaker Heights, OH (US); **Mahdi Orooji**, Cleveland, OH (US); **Mirabela Rusu**, Cleveland, OH (US); **Philip Linden**, Pepper Pike, OH (US); **Robert Gilkeson**, Cleveland Heights, OH (US); **Nathaniel Mason Braman**, Cleveland, OH (US)

(21) Appl. No.: **15/226,124**

(22) Filed: **Aug. 2, 2016**

Related U.S. Application Data

(60) Provisional application No. 62/201,837, filed on Aug. 6, 2015.

Publication Classification

(51) **Int. Cl.**

G06T 11/00	(2006.01)
G06T 7/40	(2006.01)
G06T 7/60	(2006.01)
G06K 9/46	(2006.01)
G06K 9/62	(2006.01)
G01R 33/56	(2006.01)
A61B 5/08	(2006.01)
A61B 6/00	(2006.01)
A61B 5/055	(2006.01)
A61B 5/00	(2006.01)
A61B 10/00	(2006.01)
G06T 7/00	(2006.01)
A61B 6/03	(2006.01)

(52) **U.S. Cl.**

CPC ***G06T 11/003*** (2013.01); ***G06T 7/0012*** (2013.01); ***G06T 7/0085*** (2013.01); ***G06T 7/40*** (2013.01); ***G06T 7/604*** (2013.01); ***G06K 9/46*** (2013.01); ***G06K 9/6267*** (2013.01); ***A61B 6/032*** (2013.01); ***A61B 5/08*** (2013.01); ***A61B 6/5217*** (2013.01); ***A61B 5/055*** (2013.01); ***A61B 5/4312*** (2013.01); ***A61B 5/7267*** (2013.01); ***A61B 10/0041*** (2013.01); ***G01R 33/5601*** (2013.01); *G06T 2207/10096* (2013.01); *G06T 2207/20144* (2013.01); *G06T 2207/30064* (2013.01); *G06T 2207/30068* (2013.01)

(57) **ABSTRACT**

Methods, apparatus, and other embodiments associated with classifying a region of tissue using textural analysis are described. One example apparatus includes an image acquisition logic that acquires an image of a region of tissue demonstrating cancerous pathology, a delineation logic that distinguishes nodule tissue within the image from the background of the image, a perinodular zone logic that defines a perinodular zone based on the nodule, a feature extraction logic that extracts a set of features from the image, a probability logic that computes a probability that the nodule is benign or that the nodule will respond to a treatment, and a classification logic that classifies the nodule tissue based, at least in part, on the set of features or the probability. A prognosis or treatment plan may be provided based on the classification of the image.

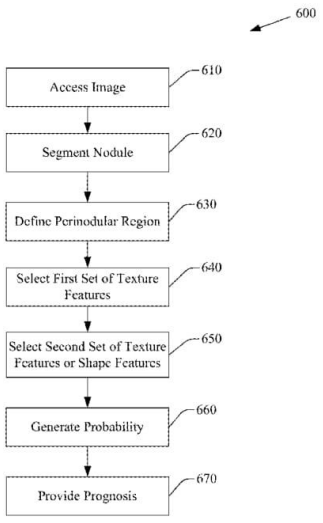

US 20170351939A1

(19) **United States**

(12) **Patent Application Publication** (10) **Pub. No.: US 2017/0351939 A1**

Madabhushi et al. (43) **Pub. Date: Dec. 7, 2017**

(54) **PREDICTING RESPONSE TO PEMETREXED CHEMOTHERAPY IN NON-SMALL CELL LUNG CANCER (NSCLC) WITH BASELINE COMPUTED TOMOGRAPHY (CT) SHAPE AND TEXTURE FEATURES**

(71) Applicant: **Case Western Reserve University**, Cleveland, OH (US)

(72) Inventors: **Anant Madabhushi**, Shaker Heights, OH (US); **Vamsidhar Velcheti**, Pepper Pike, OH (US); **Mahdi Orooji**, Cleveland, OH (US); **Sagar Rakshit**, Gurgaon (IN); **Mehdi Alilou**, Cleveland, OH (US); **Niha Beig**, Cleveland Heights, OH (US)

(21) Appl. No.: **15/612,467**

(22) Filed: **Jun. 2, 2017**

Related U.S. Application Data

(60) Provisional application No. 62/345,960, filed on Jun. 6, 2016.

Publication Classification

(51) **Int. Cl.**

G06K 9/62	(2006.01)
G01N 15/14	(2006.01)
G06T 7/11	(2006.01)
G01N 33/483	(2006.01)
A61K 39/00	(2006.01)
A61B 6/00	(2006.01)
A61B 6/03	(2006.01)
G06T 7/00	(2006.01)

(52) **U.S. Cl.**

CPC ***G06K 9/6269*** (2013.01); ***G06T 7/11*** (2017.01); ***G01N 15/14*** (2013.01); *G06T 2207/10028* (2013.01); *G06T 7/0012* (2013.01); *A61K 39/0011* (2013.01); *A61B 6/466* (2013.01); *A61B 6/03* (2013.01); *G06T 2207/30081* (2013.01); *G06T 2207/30061* (2013.01); *G01N 33/4833* (2013.01)

(57) **ABSTRACT**

Methods, apparatus, and other embodiments predict response to pemetrexed based chemotherapy. One example apparatus includes an image acquisition circuit that acquires a radiological image of a region of tissue demonstrating NSCLC that includes a region of interest (ROI) defining a tumoral volume, a peritumoral volume definition circuit that defines a peritumoral volume based on the boundary of the ROI and a distance, a feature extraction circuit that extracts a set of discriminative tumoral features from the tumoral volume, and a set of discriminative peritumoral features from the peritumoral volume, and a classification circuit that classifies the ROI as a responder or a non-responder using a machine learning classifier based, at least in part, on the set of discriminative tumoral features and the set of discriminative peritumoral features.

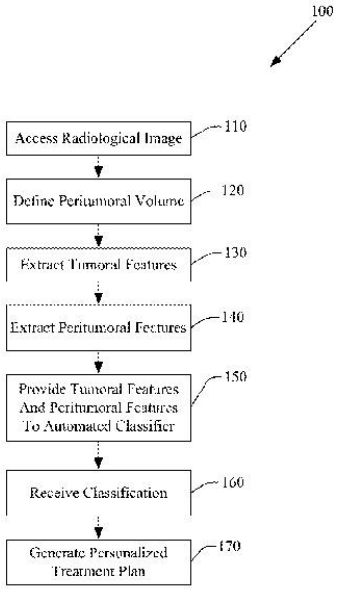

US 20170352157A1

(19) **United States**

(12) **Patent Application Publication** (10) **Pub. No.: US 2017/0352157 A1**

Madabhushi et al. (43) **Pub. Date: Dec. 7, 2017**

(54) **COMPUTERIZED ANALYSIS OF COMPUTED TOMOGRAPHY (CT) IMAGERY TO QUANTIFY TUMOR INFILTRATING LYMPHOCYTES (TILS) IN NON-SMALL CELL LUNG CANCER (NSCLC)**

(71) Applicant: **Case Western Reserve University**, Cleveland, OH (US)

(72) Inventors: **Anant Madabhushi**, Shaker Heights, OH (US); **Vamsidhar Velcheti**, Pepper Pike, OH (US); **Mahdi Orooji**, Cleveland, OH (US); **Sagar Rakshit**, Gurgaon (IN); **Mehdi Alilou**, Cleveland, OH (US); **Niha Beig**, Cleveland Heights, OH (US)

(21) Appl. No.: **15/613,751**

(22) Filed: **Jun. 5, 2017**

Related U.S. Application Data

(60) Provisional application No. 62/345,965, filed on Jun. 6, 2016.

Publication Classification

(51) **Int. Cl.**
G06T 7/00 (2006.01)
G06T 7/11 (2006.01)

(52) **U.S. Cl.**
CPC ***G06T 7/0012*** (2013.01); ***G06T 7/11*** (2017.01); *G06T 2207/10081* (2013.01); *G06T 2207/30061* (2013.01); *G06T 2207/20081* (2013.01)

(57) **ABSTRACT**

Methods, apparatus, and other embodiments predict tumor infiltrating lymphocyte (TIL) density from pre-surgical computed tomography images of a region of tissue demonstrating non-small cell lung cancer (NSCLC). One example apparatus includes a set of circuits that includes an image acquisition circuit that accesses a radiological image of a region of tissue demonstrating cancerous pathology, where the radiological image has a plurality of pixels, and where the radiological image includes an annotated region of interest (ROI), a feature extraction circuit that extracts a set of radiomic features from the ROI, where the set of radiomic features includes at least two texture features and at least one shape feature, and a classification circuit that comprises a machine learning classifier that classifies the ROI as high tumor infiltrating lymphocyte (TIL) density, or low TIL density, based, at least in part, on the set of radiomic features.